

Molecular models of alginic acid: Interactions with calcium ions and calcite surfaces

Thomas D. Perry IV ^{a,*}, Randall T. Cygan ^b, Ralph Mitchell ^a

^a *Harvard University, Division of Engineering and Applied Sciences, Cambridge, MA 02138, USA*

^b *Sandia National Laboratories, Albuquerque, NM 87185-0754, USA*

Received 29 September 2005; accepted in revised form 10 April 2006

Abstract

Cation binding by polysaccharides is observed in many environments and is important for predictive environmental modeling, and numerous industrial and food technology applications. The complexities of these cation-organic interactions are well suited for predictive molecular modeling and the analysis of conformation and configuration of polysaccharides and their influence on cation binding. In this study, alginic acid was chosen as a model polymer system and representative disaccharide and polysaccharide subunits were developed. Molecular dynamics simulation of the torsion angles of the ether linkage between various monomeric subunits identified local and global energy minima for selected disaccharides. The simulations indicate stable disaccharide configurations and a common global energy minimum for all disaccharide models at $\Phi = 274 \pm 7^\circ$, $\Psi = 227 \pm 5^\circ$, where Φ and Ψ are the torsion angles about the ether linkage. The ability of disaccharide subunits to bind calcium ions and to associate with the (10 $\bar{1}$ 4) surface of calcite was also investigated. Molecular models of disaccharide interactions with calcite provide binding energy differences for conformations that are related to the proximity and residence densities of the electron-donating moieties with calcium ions on the calcite surface, which are controlled, in part, by the torsion of the ether linkage between monosaccharide units. Dynamically optimized configurations for polymer alginate models with calcium ions were also derived.

© 2006 Elsevier Inc. All rights reserved.

1. Introduction

Modeling and prediction of cation binding as determined by polysaccharide structure is desirable for a variety of industrial applications that require the dissolution of metal-bearing minerals (Moore et al., 1972; Jamialahmadi and Mullersteinhagen, 1991), and is important for understanding cation binding in the environment and geochemical speciation-transport modeling. Calcite (calcium carbonate) mineralization (dissolution and precipitation) is important in biological, environmental, and industrial systems. In the environment, calcite is an important reservoir of carbon, and accelerated dissolution of calcite affects global carbon cycling (Schlesinger, 1997), the chemistry of marine systems (Pilson, 1998), and the local pH and

alkalinity of terrestrial environments (Stumm and Morgan, 1996). Calcite and other carbonate phases are the primary pH buffer in many natural waters, and calcite weathering impacts porosity and heterogeneity in aquifers, which, in turn, leads to hydrologic complexity in reactive transport modeling (Stumm, 1992). In terrestrial environments calcite dissolution partially regulates the fate and transport of anthropogenic pollutants, especially heavy metals (Reeder et al., 2001). In industrial systems, calcite scale develops on water pipes and can reduce heat-transfer efficiency dramatically (Stahl et al., 2000).

Interaction of biogenic species, including polysaccharides (Thomas et al., 1993; Welch and Vandevivere, 1994), with the calcite surface has been observed to affect dissolution and precipitation rates (Stumm and Morgan, 1996; Pilson, 1998). The distinctive dissolution effects of biogenic ligands depend strongly on their chemistry but an atomistic understanding of these organic–mineral interactions remains elusive. In continental environments,

* Corresponding author. Fax: +1 617 496 1471.

E-mail address: tperry@deas.harvard.edu (T.D. Perry).

polysaccharides are the second most abundant organic species following humic substances and can range in concentration from 5% to 30% of the total organic matter (Martin, 1971). Many of these compounds are extracellular polysaccharides (EPS) produced in microbial biofilms—thin films of microorganisms, including bacteria, Archaea, cyanobacteria, algae, fungi, and lichens, growing on surfaces in an excreted layer of polysaccharide (Christensen and Charaklis, 1990; Saiz-Jimenez, 1999).

Alginic acid was selected as a model environmental polysaccharide due to its demonstrated presence in the environment and well-characterized chemistry. It is a straight-chain, hydrophilic, colloidal, polyuronic acid typically arranged in three combinations of disaccharide subunits: α -L-(1–4) guluronic–guluronic (*GG*), α -L-(1–4) mannuronic–guluronic (*MG*), β -D-(1–4) mannuronic–mannuronic (*MM*). Henceforth, the subunits will be referred to as *GG*, *MG*, and *MM*. The guluronic–mannuronic disaccharide also exists but was excluded from the present study. Approximately 20–50% of polysaccharides produced in a wide sampling of marine and terrestrial bacteria were uronic acids (Kennedy and Sutherland, 1987). Alginic acid is a dominant environmental polymer produced by seaweed in marine environments (Davis et al., 2003), and by environmental bacteria including *Azotobacter vinelandii* and *Pseudomonas aeruginosa* (Boyd and Chakrabarty, 1995), which is a ubiquitous environmental bacterium (Hardalo and Edberg, 1997; Wolfgang et al., 2003). There are structural differences between alginates produced by algae and bacteria, including the relative ratios and arrangements of the different monosaccharide blocks and acetylation at the C-2 and C-3 positions of the bacterial alginate (Lattner et al., 2003).

Empirical studies have demonstrated that the electron-donating moieties of alginic acid polymers are responsible for chelating aqueous cations such as Ca^{2+} (Davis et al., 2003). Alginic acid specifically interacts with crystallographic features of calcite (Didymus et al., 1993; Perry et al., 2004) and can increase the dissolution rate of calcite (Perry et al., 2004) and other minerals (Welch et al., 1999). The electron-donating moieties of alginic acid, including all of the negatively charged oxygen atoms in the disaccharides, namely, hydroxyl oxygens, ether oxygens, and carboxylate oxygens, chelate aqueous cations (Figure 1 of Davis et al., 2003) at intermediate to high pH conditions. The carboxylate functional groups of *GG*-blocks have appropriate spacing and geometry for cation binding (Dheu-Andries and Pérez, 1983), and *GG*-blocks have a higher affinity for divalent cation binding than their *MM* counterparts (Smidsrød and Haug, 1965). As a result, the proportion of *MM*- and *GG*-blocks and their macromolecular conformation determine the physical properties and the affinity of the polymer for cation binding (Haug et al., 1967). Cation binding can be ordered or disordered (Braccini and Pérez, 2001) as determined by the proportion of *GG*- and *MM*-blocks and their macromolecular conformation (Haug et al., 1967). Planar *MM*-blocks also bind

calcium ions, although the association is less ordered than for *GG* because they do not have the correct special and geometric arrangement for binding sites (Grant et al., 1973).

Cation binding and gelling of alginic acid are important aspects of this biogenic macromolecule. A detailed molecular level understanding of the complex chemical contributions to cation binding is essential to fully comprehend these phenomena. The use of molecular modeling methods such as energy optimization and molecular dynamics in this study allows access to additional insights that may be difficult, if nearly impossible, to obtain experimentally (Guimarães et al., 2004) and ultimately broadens the understanding of these chemical interactions. Also, a fundamental understanding of the atomistic interactions of organic species with mineral surfaces during dissolution and precipitation needs to be developed (Banfield et al., 1999; Welch and Vandevivere, 1994). Predictive molecular simulation requires development of empirical energy force fields that can accurately simulate inter- and intra-molecular interactions in complex, heterogeneous systems with different and numerous molecular types (Kollman, 1996). Previous modeling efforts have been limited by the availability of an energy force field that can simultaneously simulate these complicated systems, especially those involving a hydrated organic–inorganic interface (de Leeuw et al., 1998, 2004; Hwang et al., 2001; Cormack et al., 2004; Duffy and Harding, 2004). Attempts to model different aspects of these systems have been performed using static calculations (de Leeuw and Cooper, 2004), in vacuo (Duckworth et al., 2003), by focusing on the interaction of organics with cations (Braccini et al., 1999) and water (Guimarães et al., 2004), by modeling mineral surfaces with monolayers of water (Kerisit and Parker, 2004a), or by combination of force field models (de Leeuw and Cooper, 2004).

This study presents a comprehensive approach for determination of disaccharide and polysaccharide structure as determined by monosaccharide configuration and conformation. Structural stability is examined in the presence of calcium cations and at elevated temperature. Using a newly developed force field, the structures and energetics of these organic materials are evaluated with and without a calcite surface. The approach and results will be of interest to computational and environmental chemists and geochemists.

2. Modeling approach

2.1. Polymer structure

Schematic representations of the three primary polymeric subunits of alginic acid used in the molecular simulations are shown in Fig. 1. These structures are empirically confirmed in several independent analyses of natural alginic acid (Evans and Linker, 1973). The conformations of disaccharides are largely defined by two torsion

angles linking the sugar rings: $\Phi = \text{O}^{5'} \rightarrow \text{C}^{1'} \rightarrow \text{O}^4 \rightarrow \text{C}^4$ and $\Psi = \text{C}^{1'} \rightarrow \text{O}^4 \rightarrow \text{C}^4 \rightarrow \text{C}^5$ (Fig. 1) (Braccini et al., 1999).

2.2. Computational chemistry basis

2.2.1. Study of alginic acid configuration using CVFF

The consistent valence force field (CVFF) was originally designed for investigating peptide and protein structures (Dauber-Osguthorpe et al., 1988) but recently has been successfully applied to polysaccharides (Hoog et al., 2002) and to organic macromolecule–calcium ion interactions (Iyer and Qasba, 1999). CVFF describes the energy of a chemical system through summation of individual interatomic energies and the geometry of the molecular configuration (Cygan, 2001). The energy values reported in this study are based on the potential models within CVFF and can be used to interpret relative conformational stability but are not necessarily absolute quantities. The bonded terms usually dominate the structure determination of neutral organic molecules, while the nonbonded terms become increasingly important in charged or polar systems, including the simulation of calcium ion–alginate disaccharides and polymer systems. This force field was used to analyze alginic acid structure in the absence and presence of free calcium cations. Electronic structure calculations were also completed to validate the CVFF-derived structures and energies associated with the optimized disaccharide acids, anions, and calcium complexes.

2.2.2. Study of alginic acid in the presence of calcite using a new hybrid force field

The CVFF force field was not designed for simulating crystalline materials such as the bulk and surface structures of calcite. Hence, a new force field was developed with optimized interatomic potentials for organic molecule interaction with a carbonate mineral surface with explicit water molecules to represent a hydrated environment. We had previously developed an accurate energy force field capable of simulating a carbonate mineral surface with partial and full water hydration. Further development of the force field for the present study allowed inclusion of interaction parameters for the organic

components of the alginic acid units. Atom typing and descriptions (Table 1), expressions for hybrid force field functionality (Table 2), and parameters for the carbonate–water–organic interactions (Table 3) are summarized. Parameters for the organic components are taken from the CVFF force field (Dauber-Osguthorpe et al., 1988). Van der Waals interactions presented in Table 3 were derived through the use combination rules (Halgren, 1992) and the conversion of Buckingham style potentials (Duckworth et al., 2003) to the more conventional Lennard–Jones potential (see Table 2).

2.3. Computational methods

2.3.1. Conformational analysis of disaccharides and polysaccharides

All atomistic simulations were performed using Cerius² software (Accelrys Inc., San Diego, CA). Molecular geometries were obtained through energy minimization procedures based on an energy convergence value of 0.001 kcal mol⁻¹. Disaccharide conformations are determined primarily by the torsion of linkages between monomers and computer experiments investigated the local and global energy minima of the disaccharides as primarily determined by linkage torsions. The two principal torsion angles (Φ , Ψ) were rotated 360° simultaneously at 10°

Table 1
Force field and atom types and descriptions

Element	Description	Symbol	Charge (e)
H	Water hydrogen	<i>h*</i>	0.4100
O	Water oxygen	<i>o*</i>	-0.8200
O	Carbonate oxygen	<i>o</i>	-1.1145
C	Carbonate carbon	<i>c</i>	1.3435
Ca	Calcium	<i>Ca</i>	2.0000
H	Alkane hydrogen	<i>h</i>	0.1000
H	Hydroxyl hydrogen	<i>ho</i>	0.3500
C	Alkane carbon	<i>c1</i>	-0.0700
C	Carboxyl carbon	<i>c'</i>	0.4100
C	Carboxylate carbon	<i>c⁻</i>	0.1400
O	Ether oxygen	<i>oe</i>	-0.3000
O	Carboxyl oxygen	<i>o'</i>	-0.3800
O	Carboxylate oxygen	<i>o⁻</i>	-0.5700
O	Hydroxyl oxygen	<i>oh</i>	-0.3800

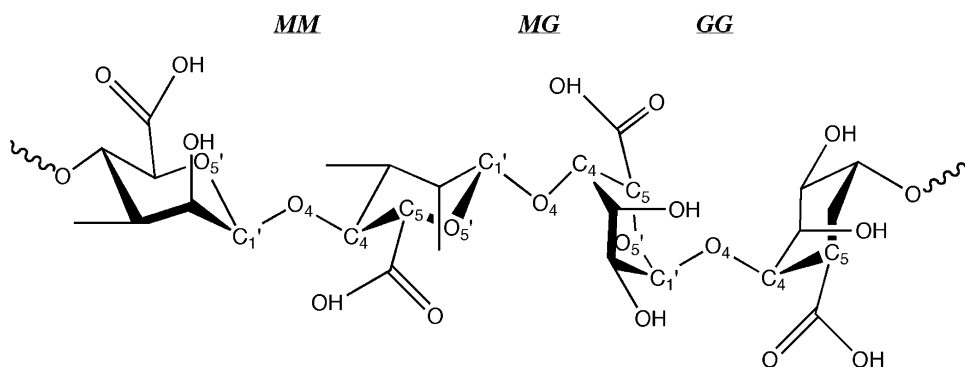


Fig. 1. Chemical structure of alginic acid.

Table 2
Expressions for hybrid force field functionality

Total energy
$E_{\text{total}} = E_{\text{Coul}} + E_{\text{VDW}} + E_{\text{bondstretch}} + E_{\text{anglebend}} + E_{\text{inversions}} + E_{\text{torsions}}$
Coulombic energy (E_{Coul})
$E_{\text{Coul}} = \frac{e^2}{4\pi\epsilon_0} \sum_{i \neq j} \frac{q_i q_j}{r_{ij}}$
van der Waals energy (E_{VDW})
$E_{\text{VDW}} = \sum_{i \neq j} D_{o,ij} \left[\left(\frac{R_{o,ij}}{r_{ij}} \right)^{12} - 2 \left(\frac{R_{o,ij}}{r_{ij}} \right)^6 \right]$
Bond stretch energy ($E_{\text{bondstretch}}$) of the hydroxyl
$E_{\text{bondstretch},ij}^{o*-h*} = \frac{1}{2} k_1 (r_{ij} - r_o)^2$
Bond stretch energy ($E_{\text{bondstretch}}$) of the carbonate
$E_{\text{bondstretch},ij}^{c-o} = D_e (e^{-\alpha(r-r_o)} - 1)^2$
Angle bend energy ($E_{\text{anglebend}}$)
$E_{\text{anglebend},ijk} = \frac{1}{2} k_2 (\theta_{ijk} - \theta_o)^2$
Bond inversion energy ($E_{\text{inversion}}$) of the carbonate
$E_{\text{inversion},ijkl} = \frac{1}{2} k_i (1 + \cos \phi)^2$
Torsion energy (E_{torsion}) of the organics
$E_{\text{torsion},ijkl} = \sum_j \left\{ \left(\frac{1}{2} k_i \right) (1 - n \cos \phi) \right\}$

increments to allow an analysis of conformational energies. For each iteration, torsional bonds were spatially fixed, the remaining atoms of the disaccharide molecule were geometrically optimized, and the total energy was calculated for all atomic interactions. Excluding the linkage torsion of interest, this approach allows complete relaxation of the molecule including all other torsion angles, including those associated with hydroxyl and carboxylate functional groups. The relatively large increments of rotation were sufficient for detecting regions of potential energy minima. Torsion angle increments as small as 0.5° we used in the exploratory Φ - Ψ potential energy map and provided results that are consistent with those obtained using the larger increments presented here. Some artifacts of the incremental shifts were observed and were attributed to the inability of the bonds, especially those of stabilizing functional groups, to continuously minimize during incremental rotation. This artifact was ameliorated by using torsional values for minima from automated analysis as a starting point for a full geometry optimization. The full optimizations were initiated with the first-order conformation derived from the automated torsional analysis but allowed full atomic flexibility, thereby allowing all atoms and bonds to relax and energy minimize.

For Coulombic and van der Waals interactions in simulations with disaccharides, a spline cutoff distance of 8.5 Å was used; for polymers, a cutoff value of 55.0 Å was employed. The rationale for modifying the cutoff values for larger molecules is to assure that intramolecular interactions between atoms are included in calculations (Allen and Tildesley, 1987), which is especially important with large polymers that can exhibit significant intramolecular interactions (Sun et al., 1998). When there were significant large energy instabilities or nonconvergence issues, those conformations were denoted by assigning an artificial

Table 3
Force field parameters for the carbonate–water–organic VDW interactions

Interacting atoms		R_o (Å)	D_o (kcal mol ⁻¹)
Species <i>i</i>	Species <i>j</i>		
<i>o*</i>	<i>o*</i>	3.5532	1.5540E-01
<i>o</i>	<i>o*</i>	4.4266	6.9687E-05
<i>o</i>	<i>o</i>	5.9000	4.5000E-08
<i>Ca</i>	<i>o*</i>	5.6000	3.4000E-04
<i>Ca</i>	<i>o</i>	4.9460	1.4555E-03
<i>h</i>	<i>o*</i>	3.1516	7.6845E-02
<i>h</i>	<i>o</i>	4.0250	3.4460E-05
<i>h*</i>	<i>o</i>	4.0250	3.4460E-05
<i>ho</i>	<i>o</i>	4.0250	3.4460E-05
<i>h</i>	<i>Ca</i>	3.6710	1.6051E+00
<i>c</i>	<i>o*</i>	3.8066	1.5165E-01
<i>c1</i>	<i>o*</i>	3.9516	7.7850E-02
<i>c1</i>	<i>o</i>	4.8250	3.4911E-05
<i>c1</i>	<i>Ca</i>	4.4710	1.6261E+00
<i>c1</i>	<i>h</i>	3.4587	3.8497E-02
<i>c1</i>	<i>c1</i>	4.3500	3.9000E-02
<i>c'</i>	<i>o*</i>	3.8066	1.5165E-01
<i>c'</i>	<i>o</i>	4.6800	6.8007E-05
<i>c'</i>	<i>Ca</i>	4.3260	3.1676E+00
<i>c'</i>	<i>h</i>	3.3414	7.4993E-02
<i>c'</i>	<i>c1</i>	4.2025	7.5974E-02
<i>c'</i>	<i>c'</i>	4.0600	1.4800E-01
<i>c⁻</i>	<i>o*</i>	3.8066	1.5165E-01
<i>c⁻</i>	<i>o</i>	4.6800	6.8007E-05
<i>c⁻</i>	<i>Ca</i>	4.3260	3.1676E+00
<i>c⁻</i>	<i>h</i>	3.3414	7.4993E-02
<i>c⁻</i>	<i>c1</i>	4.2025	7.5974E-02
<i>c⁻</i>	<i>c'</i>	4.0600	1.4800E-01
<i>c⁻</i>	<i>c⁻</i>	4.0600	1.4800E-01
<i>oe</i>	<i>o*</i>	3.3816	1.8823E-01
<i>oe</i>	<i>o</i>	4.2550	8.4410E-05
<i>oe</i>	<i>Ca</i>	3.9010	3.9316E+00
<i>oe</i>	<i>h</i>	2.9711	9.3081E-02
<i>oe</i>	<i>c1</i>	3.7368	9.4297E-02
<i>oe</i>	<i>c'</i>	3.6101	1.8370E-01
<i>oe</i>	<i>c⁻</i>	3.6101	1.8370E-01
<i>oe</i>	<i>oe</i>	3.2100	2.2800E-01
<i>o'</i>	<i>o*</i>	3.3816	1.8823E-01
<i>o'</i>	<i>o</i>	4.2550	8.4410E-05
<i>o'</i>	<i>Ca</i>	3.9010	3.9316E+00
<i>o'</i>	<i>h</i>	2.9711	9.3081E-02
<i>o'</i>	<i>c1</i>	3.7368	9.4297E-02
<i>o'</i>	<i>c'</i>	3.6101	1.8370E-01
<i>o'</i>	<i>c⁻</i>	3.6101	1.8370E-01
<i>o'</i>	<i>oe</i>	3.2100	2.2800E-01
<i>o'</i>	<i>o'</i>	3.2100	2.2800E-01
<i>o⁻</i>	<i>o*</i>	3.3816	1.8823E-01
<i>o⁻</i>	<i>o</i>	4.2550	8.4410E-05
<i>o⁻</i>	<i>Ca</i>	3.9010	3.9316E+00
<i>o⁻</i>	<i>h</i>	2.9711	9.3081E-02
<i>o⁻</i>	<i>c1</i>	3.7368	9.4297E-02
<i>o⁻</i>	<i>c'</i>	3.6101	1.8370E-01
<i>o⁻</i>	<i>c⁻</i>	3.6101	1.8370E-01
<i>o⁻</i>	<i>oe</i>	3.2100	2.2800E-01
<i>o⁻</i>	<i>o'</i>	3.2100	2.2800E-01
<i>o⁻</i>	<i>o⁻</i>	3.2100	2.2800E-01
<i>oh</i>	<i>o*</i>	3.3816	1.8823E-01
<i>oh</i>	<i>o</i>	4.2550	8.4410E-05
<i>oh</i>	<i>Ca</i>	3.9010	3.9316E+00
<i>oh</i>	<i>h</i>	2.9711	9.3081E-02
<i>oh</i>	<i>c1</i>	3.7368	9.4297E-02
<i>oh</i>	<i>c'</i>	3.6101	1.8370E-01
<i>oh</i>	<i>c⁻</i>	3.6101	1.8370E-01

(continued on next page)

Table 3 (continued)

Interacting atoms		R_o (Å)	D_o (kcal mol ⁻¹)
Species <i>i</i>	Species <i>j</i>		
<i>oh</i>	<i>oe</i>	3.2100	2.2800E-01
<i>oh</i>	<i>o'</i>	3.2100	2.2800E-01
<i>oh</i>	<i>o⁻</i>	3.2100	2.2800E-01
<i>oh</i>	<i>oh</i>	3.2100	2.2800E-01

energy value of +1000 kcal mol⁻¹. The previously successfully minimized conformation model was then reloaded and automatically advanced to the next simulation torsion angle increment to continue with the Φ - Ψ energy mapping. Reloading the previous model was important to lessen the effects of instability created by spatial rearrangements during the previous energy minimization, such as those involving the rearrangements of the torsions of the carboxylate. These potential energy map simulations were repeated with protonated and deprotonated (charge states of 0 and -2, respectively) *MM*, *GG*, and *MG* disaccharides and with dielectric constant (ϵ) values set at either 1 or 78. Calculations performed with $\epsilon = 1$ represent a vacuum environment where the Coulombic interactions are evaluated directly. Increasing the dielectric constant ($\epsilon = 78$) in the simulations effectively shields the intramolecular Coulombic interactions and mimics an aqueous environment where water molecules implicitly solvate the molecule (Guenot and Kollman, 1992). We accept the approximation that exists for calculations at $\epsilon = 78$ due to the enhanced shielding of the 1–4 carbon interactions, which are of interest when modeling torsions (Braccini et al., 1999). However, this is not a critical concern because we are attempting to evaluate the conformation resulting in the lowest potential energy, i.e. the most stable conformation. At the dielectric values evaluated, the potential wells remain in the same position and are relatively unchanged, except in breadth and depth, which does not affect the region of determined stable conformation. Polymers were constructed from the resulting stable conformations of the disaccharides and molecular dynamics simulations were conducted, as described below.

For calculation of energy minima when the disaccharides bind with calcium ion, identified stable structures of deprotonated disaccharides as first determined above were manually docked with a cation and energetically minimized with $\epsilon = 1$. These simulations were performed on the isolated gas-phase model to identify first-order effects and determine if the binding of calcium can influence saccharide structure; detailed modeling should necessarily include explicit hydration, since the water molecules affect cation binding and competition with any aqueous phase. Relative stability of various configurations was assessed by manually interacting the calcium ion with different parts of the disaccharide. Additionally, short duration molecular dynamics simulations (less than 10 ps) were employed to evaluate relative stabilities. Following molecular dynamics simulations and conformation verification, polymers were constructed from calcium-associated disaccharides and

these 20-unit polysaccharides were subsequently energy-minimized.

Electronic structure calculations of several disaccharide systems were completed using the density functional code DMol³ (Delley, 1990, 2000). Optimized all-electron configurations were obtained for the protonated and deprotonated *MM*, *GG*, and *MG* structures and for the associated Ca²⁺ complexes. Calculations incorporated the nonlocal gradient-corrected or generalized gradient approximation, with double numerical plus polarization functionals to ensure a proper description of internal hydrogen bonding (Perdew and Wang, 1992). Iteration of the wave equations to a self-consistent field solution required an energy difference of less than 0.0063 kcal/mol. Energy-minimized structures were derived through a series of steepest descent, conjugate gradient, and Newton–Raphson methods allowing all atoms to relax during the optimization. An energy convergence criteria of 0.013 kcal/mol was used for the geometry optimization.

2.3.2. Molecular dynamics simulations of disaccharides and polysaccharides cluster models

Molecular dynamics calculations were performed on the various disaccharides and on constructed 20-unit polysaccharides. All dynamics simulations were performed as canonical ensembles where volume and temperature conditions were maintained statistically constant (Allen and Tildesley, 1987). A Nosé–Hoover thermostat (Hoover, 1985) maintained at 300 K was used to control temperature during the simulations, which were performed for periods of 100 ps with a relaxation time of 0.1 ps. The duration of these simulations is adequate to completely sample their conformational space; the molecules maintain the representative conformations associated with potential energy minima. The Verlet velocity algorithm was used to obtain accurate integration of the dynamics equations and statistical ensembles (Verlet, 1967). Polysaccharides were additionally subjected to an initial 20 ps equilibration run before the long-term simulation to ensure full equilibration of the system. A more detailed study of the interaction of the polysaccharides with calcium ions would necessarily include model simulations with more than a single polysaccharide chain; the present study, however, limited this effort to emphasize the interactions of alginic acid with the calcite surface.

Molecular modeling of the structural conformations of the disaccharides identified global energy minimum (*a*) and local energy minimum (*b*) conformations, and those results are employed in the remainder of this study.

2.3.3. Simulation of disaccharides in the presence of a (10 $\bar{1}$ 4) calcite surface

The total dimensions of the simulation cell with periodic boundary conditions were 24.0 × 29.7 × 56.8 Å and consisted of an approximated 30 Å-thick solvation region above a 20 Å-thick substrate originally created from the (10 $\bar{1}$ 4) cleavage of calcite and the experimental crystal structure

(Effenberger et al., 1981). All simulations contain the identical number of atoms and therefore potential energies, relative binding enthalpies, and stable configurations can be directly compared. Disaccharides are treated as dianionic species with the carboxylic groups deprotonated in order to represent the expected protonation state at neutral pH conditions (Belitz and Grosch, 1987). The dimensions of the simulation cell were important for minimizing interactions among periodic images of the reference cell. Periodic simulations were performed using spline cutoffs of 8 and 8.5 Å for the short-range van der Waals interactions and long-range Ewald sums for Coulombic interactions (Tosi, 1964). The molecular simulation methods were used for the periodic simulations. Due to the charged nature of the disaccharide anions, a compensating background charge is applied across the simulation cell to maintain neutrality. Systematically rotating and moving the disaccharide in the z -axis direction determined disaccharide starting orientation and distance from the surface with the lowest energy. Simulations were allowed to equilibrate using a 1 fs time step for an initial 20 ps period followed by a 50 ps production period for obtaining equilibrium statistics on energy and structure. Results for the MM - b simulations are derived from the last stages of the 20 ps equilibration run due to transient instabilities in the 50 ps production run.

Disaccharides in solvated and surface-sorbed (surficial) systems were compared based on simulation results for sorption energies and ether-linkage torsions. Sorption energies (E_{sorp}) were calculated for each of the disaccharides according to the following:

$$E_{\text{sorp}} = E_{\text{solv}} - E_{\text{surf}}, \quad (1)$$

where E_{solv} is the mean potential energy of the system when the disaccharide is solvated (far removed from the calcite–solution interface) and E_{surf} is the mean potential energy of the system when the disaccharide is located at the mineral surface with no intermediate water molecules (Fig. 2) from the 50 ps simulations.

Results for molecular ordering and energetics at the calcite–water interface are presented in this study. Selected monolayers of calcite components (Ca^{2+} and CO_3^{2-} and water were analyzed by quantifying the variation in density of constituent calcite atoms 3 Å into the calcite surface and water/disaccharide atoms 3.5 Å into the bulk solution. A complete data set is presented for the simulation of the GG disaccharide–calcite system. Similar simulations were conducted with the MG and MM disaccharides with calcite and are summarized and compared, but detailed presentation of the data has been omitted for brevity.

3. Results and discussion

The following sections explore the energetics and torsion mechanics of alginic acid disaccharide subunits rotated about the ether linkage. Molecular dynamics simulations are mapped onto the potential energy surfaces to identify potential metastable conformations. Calcium binding of

the geometry-optimized disaccharides was explored by the manual docking of calcium ion at binding sites of the various disaccharides. Minimized Ca^{2+} -disaccharide structures were then used to predict possible conformations of the Ca^{2+} -polymer complex. The determined structures of the alginic acid disaccharides were then interacted using explicit hydration at near (sorbed) and far (solvated) distances from a simulated (10 $\bar{1}$ 4) calcite surface and torsional behavior was observed during dynamics simulation. Finally, a disaccharide was interacted with a surface defect on the (10 $\bar{1}$ 4) calcite surface.

3.1. Torsional conformation of disaccharides

Alginic acid is produced in MM , GG , and alternating MG blocks. The different linkages between the monomers are the primary control on polymer structure, and torsion simulations were implemented to determine stable conformations of MM , GG , and MG disaccharides when protonated and deprotonated. The minimum (a) structure is defined as the global potential energy minimum for a particular disaccharide for the experimental conditions. Metastable local minima are assigned alphabetically (b , c , d) as energy increases (Table 4). In this study, the neutral disaccharides have functional groups completely protonated, while the deprotonated disaccharides are represented by removal of the hydrogen from the carboxylic acid groups to form charged carboxylate anions. The effects of deprotonated hydroxyl groups are not studied here due to their relatively high pK_a compared to the carboxylate groups ($\text{pK}_a = 3.4\text{--}4.4$) (Belitz and Grosch, 1987). However, the hydroxyls do play an important role in stabilization of the configurations of the disaccharides and respond to movements of the disaccharides, and especially act to stabilize the carboxylate groups by hydrogen bonding. Potential energy values in all plots are normalized with the lowest energy conformation as

$$E_{\text{plot}} = E_{\text{measured}} - E_{\text{minimum}} \quad (2)$$

for each of the disaccharides. Absolute potential energy values for each minimum are available in Table 4. The contour plots of measured potential energies (kcal mol^{-1}) of protonated and deprotonated disaccharides at $\epsilon = 1$ and 78 provide the backgrounds of the figures highlighting dynamic molecular simulation (viz. Figs. 3–5).

MM disaccharides consistently exhibit two local minima in the torsion angle potential energy maps (Figs. 3–5), except when the disaccharide was deprotonated with $\epsilon = 1$ (Table 4). The global potential energy minimum (a) consistently was determined with an additional local minimum (b). Increasing the ϵ value causes a broadening of the minima for the protonated disaccharide. The deprotonated MM disaccharide appears to have only a single energy minimum at $\epsilon = 1$, while at $\epsilon = 78$ two local minima are observed. Presumably, the decreased torsional freedom at $\epsilon = 1$ results from interaction of the deprotonated carboxyl groups on the subunits. These interactions are electrostatic

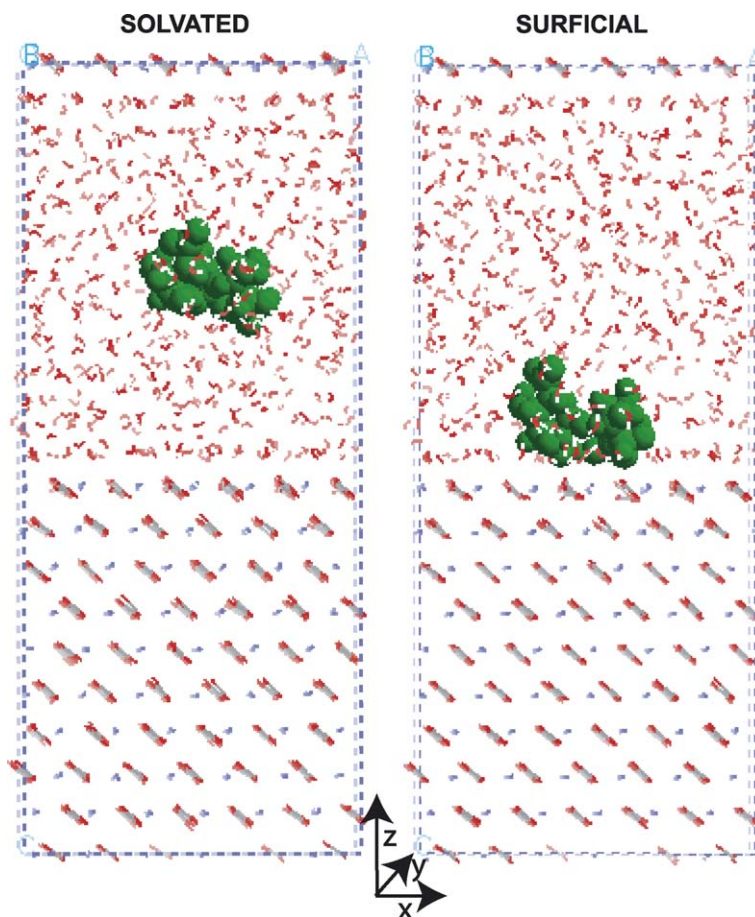


Fig. 2. Examples of periodic simulation cells of solvated and surface-sorbed systems with the *GG*-a disaccharide and the $(10\bar{1}4)$ calcite face with explicit hydration. The disaccharides have been colored green to facilitate identification.

cally shielded when $\varepsilon = 78$. The minimum *b* has a higher energy in this conformation because the carboxylates are axially eclipsed, that is, overlapping when examined along the long axis of the disaccharide, whereas they are equatorially oriented at minimum *a*. The eclipsing is more apparent at $\varepsilon = 1$ with the deprotonated disaccharide where minimum *b* occurs at $\varepsilon = 78$ because the unshielded nonbonded interactions result in high-energy conformations. This restriction does not occur with the protonated disaccharide due to the reduced charges associated with the functional groups.

Torsion maps for the *GG* disaccharide exhibit minima in the same regions as the *MM* disaccharide. The protonated *GG* disaccharide at $\varepsilon = 1$ exhibits a complex adiabatic map with four local minima (Table 4). The *GG* disaccharides have greater energy in all conformations than *MM* disaccharides (Table 4). This is likely due to their α -linkage and buckled conformation, which results in close association of interacting functional groups, in comparison to the more planar β -linkages of the *MM* disaccharides. *GG*-blocks are arranged in α -conformations with molecular repeats of 8.7 Å (Atkins et al., 1973a), while *MM* regions are β -linked with a 10.35 Å molecular repeat (Atkins

et al., 1973b), and the close association of interacting functional groups is probably responsible for the reversal of the *a* and *b* minima in *GG* compared to the *MM* torsion maps. The deprotonated *GG* disaccharide at $\varepsilon = 1$ exhibits extremely restricted torsional freedom due to the more closely spaced carboxylate groups in the α -linkage than in the β -linkage on the *MM* disaccharide, and hence more significant interactions of the eclipsing of negatively charged carboxylate groups. The α -conformation results in greater steric hindrance than the β -linked polysaccharides due to interaction of the oxygens on the carboxylate groups and decreased flexibility of the molecule (Whitting, 1971). Our findings on the torsional minima of *MM* and *GG* are in reasonable agreement with the conformations determined by Braccini, Grasso and Perez (Braccini et al., 1999).

The *MG* linkage exhibits similar torsional freedom as observed for the *MM* and *GG* disaccharides. When deprotonated with $\varepsilon = 1$, the *MG* linkage has severely limited torsional freedom relative to the *MM* and *GG* disaccharides (Fig. 5). The contrast in stabilization is less significant for the torsion maps calculated for $\varepsilon = 78$ where the implicit solvation significantly reduces the intramolecular electrostatics for the charged carboxylate groups. Nonetheless,

Table 4
Potential energy minima of torsional conformations of protonated and deprotonated alginic acid subunit disaccharides

Disaccharide	Dielectric	Minimum	Φ ($^\circ$)	Ψ ($^\circ$)	E (kcal mol $^{-1}$)	ΔE^a (kcal mol $^{-1}$)
Protonated <i>MM</i>	1	<i>a</i>	306.0	240.0	7.88	0
		<i>b</i>	28.9	248.7	8.17	0.30
	78	<i>a</i>	290.6	241.1	23.74	0
		<i>b</i>	42.5	249.2	25.86	2.12
Deprotonated <i>MM</i>	1	<i>a</i>	279.0	226.3	73.38	0
		<i>b</i>				
	78	<i>a</i>	290.7	241.2	23.85	0
		<i>b</i>	41.3	249.1	26.54	2.69
Protonated <i>GG</i>	1	<i>a</i>	53.5	244.0	20.56	0
		<i>b</i>	289.8	233.4	26.04	5.48
		<i>c</i>	194.9	204.1	28.50	7.94
		<i>d</i>	236.2	59.2	31.96	11.39
	78	<i>a</i>	291.5	238.4	37.19	0
		<i>b</i>	37.3	250.1	39.27	2.08
		<i>a</i>	276.8	253.3	64.34	0
		<i>b</i>	58.7	243.2	38.10	11.73
Deprotonated <i>GG</i>	1	<i>a</i>	276.8	253.3	64.34	0
		<i>b</i>				
	78	<i>a</i>	284.6	223.1	26.38	0
		<i>b</i>	58.7	243.2	38.10	11.73
Protonated <i>MG</i>	1	<i>a</i>	292.1	242.7	13.15	0
		<i>b</i>	40.0	244.3	15.99	2.84
	78	<i>a</i>	291.5	228.3	25.88	0
		<i>b</i>	42.8	245.3	27.87	1.99
Deprotonated <i>MG</i>	1	<i>a</i>	299.5	225.1	76.03	0
		<i>b</i>				
	78	<i>a</i>	291.6	228.3	25.77	0
		<i>b</i>	42.3	244.6	28.25	2.47

^a $\Delta E = E_{\text{measured}} - E_{\text{minimum}}$.

the mixed disaccharide exhibits similar Φ - Ψ mapping for the stable conformations at the *a* and *b* minima.

Comparison of the data for the disaccharides reveals interesting insights about the conformation of the disaccharides. For all disaccharides, except protonated *GG* with $\epsilon = 1$, the global energy minima *a* (i.e. the most stable confirmation) occurs at $\Phi \approx 270^\circ$, $\Psi \approx 240^\circ$, while the second most stable confirmation appears at $\Phi \approx 45^\circ$, $\Psi \approx 245^\circ$ (Table 4). Deprotonated disaccharides are stabilized by 15–20 kcal mol $^{-1}$ with increasing ϵ (Table 4) due to shielding of the Coulombic interactions associated with the carboxylate groups. In contrast, raising ϵ destabilizes protonated disaccharides, as demonstrated by increased potential energy values. The α -linked disaccharides generally have higher potential energy values than the more planar β -linked disaccharides because of the closer spatial arrangement of interacting functional groups and increased destabilizing interactions. The *MG* linkage can exhibit energetics similar to *GG* or *MM* linkages depending on the torsional conformation the disaccharide. The most stable conformation of Ψ among all monosaccharide constituents occurs near a torsional conformation of 240° . This defining feature is attributed to the positioning of the carboxylate group one atom away from the ether linkage on the Ψ -linkage (viz.

Fig. 1) as opposed to two atoms away on the Φ -linkage and the restricted torsional freedom controlled by this dominant functionality closely interacting with the adjacent monosaccharide.

Excellent structural agreement was observed between the energy-minimized disaccharides (protonated and deprotonated) derived from the force field and the quantum calculations. Bond distances are typically within 0.005 Å of each other with no greater than 0.03 Å difference for the largest discrepancies. Bond angles, likewise, are consistent for structures obtained using the two different modeling approaches—typically, bond angles are no more than 3° different from each other. The torsion angles associated with the ether linkage are consistent between the two methods as well. Differences in these critical linkage angles average less than 5° , and in most cases discrepancies are less than 2° . The electronic structure results validate the use of CVFF and the other atomistic-based computational methods, at least for the case of the disaccharide systems analyzed in this study. In order to better assess the stability of the various disaccharide configurations at ambient conditions and to observe any temporal variation, molecular dynamics simulations were conducted.

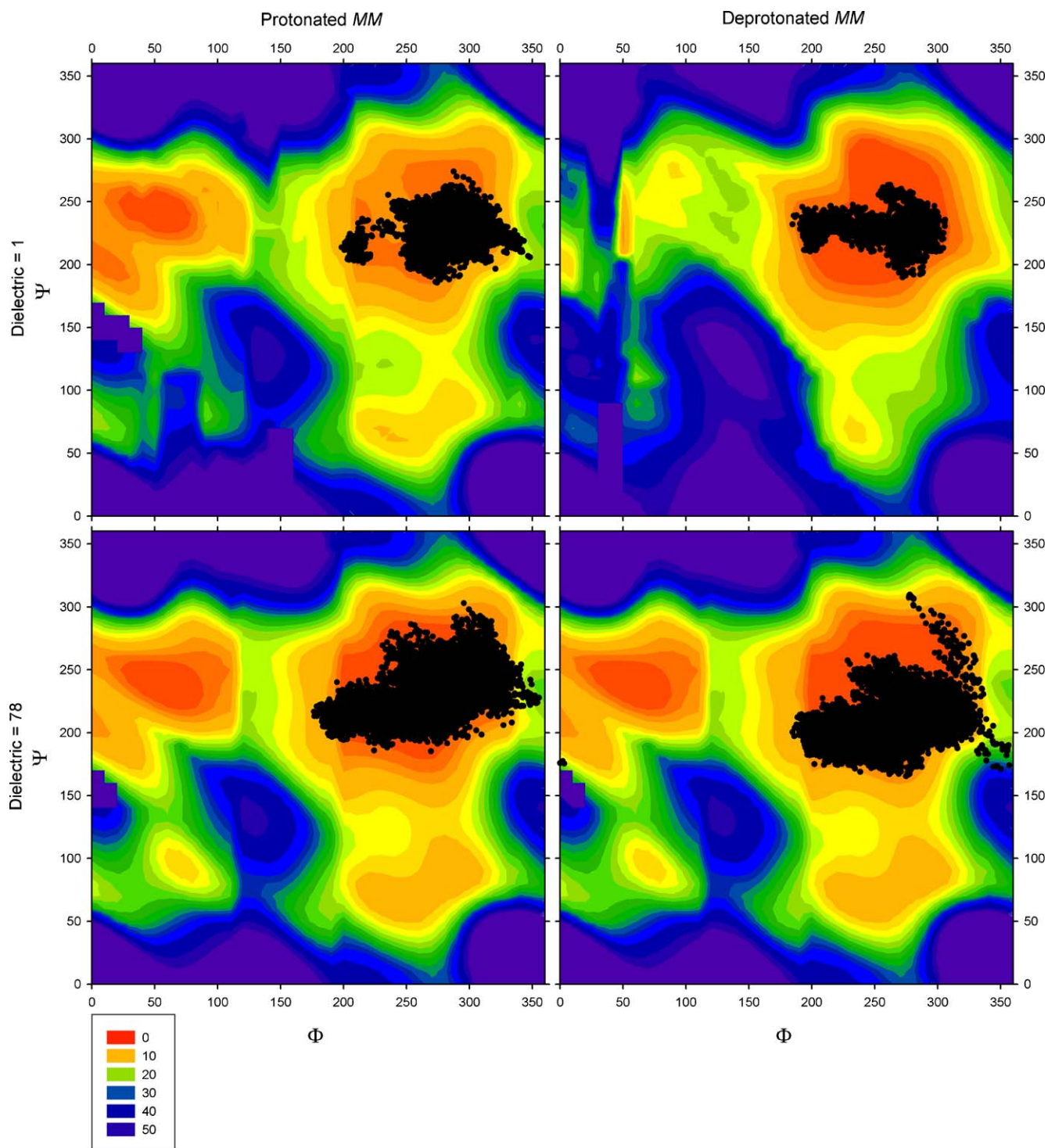


Fig. 3. Molecular dynamics simulation (100 ps) of the torsional changes of protonated and deprotonated mannuronic disaccharides (*MM*) at 300 K superimposed over contour plots of the energy minima of the disaccharide. Contours are provided in kcal mol⁻¹.

3.2. Molecular dynamics simulations with disaccharides

Molecular dynamics simulations demonstrate that *MM*, *GG*, and *MG* disaccharides are most stable near the global energy minimum (*a*) for all protonated and deprotonated disaccharides at $\epsilon = 1$ and 78, excluding the protonated *GG* disaccharide. Starting conformations for these

simulations were derived from minimized disaccharide structures with chiral centers that were empirically shown to be part of a naturally produced polymer.

The initial configuration for the *MM* linkage is at $\Phi = 206.7^\circ$, $\Psi = 217.3^\circ$. For all simulations, the disaccharide maintains its position in the potential energy trough associated with minima *a* (Fig. 3). There is some oscillation

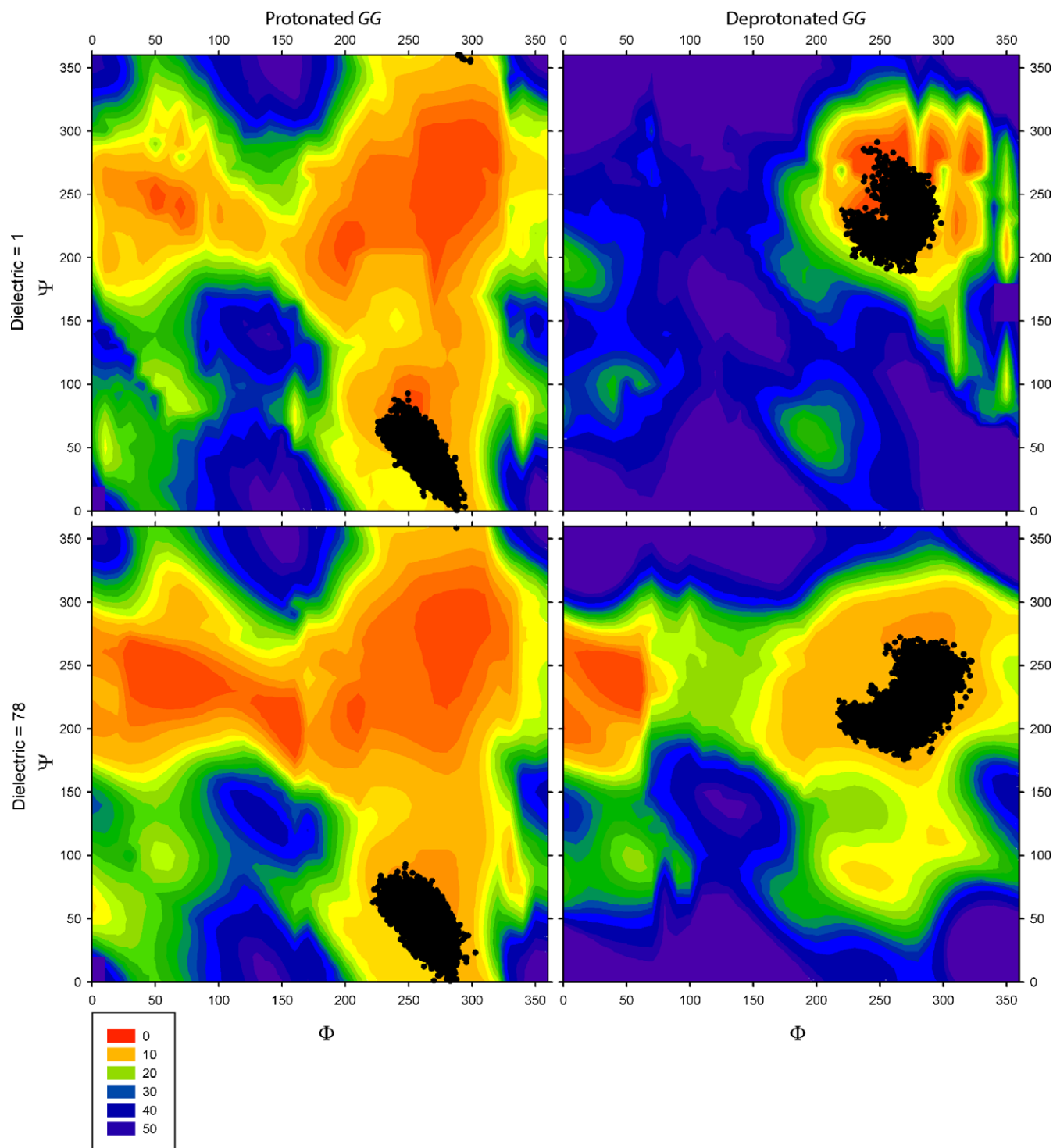


Fig. 4. Molecular dynamics simulation (100 ps) of the torsional changes of protonated and deprotonated guluronic disaccharides (*GG*) at 300 K superimposed over contour plots of the energy minima of the disaccharide. Contours are provided in kcal mol⁻¹.

of the torsion values within the trough associated with the energy minimum. The occasional blocking at potential energy barriers for certain conformations (e.g. protonated *MM*, $\epsilon = 1$, $\Phi = 0\text{--}30$, $\Psi = 150$) is the result of an energetically unfavorable conformation resulting in nonconvergence of the energy minimization calculations and data smoothing assumptions made while plotting.

Protonated *GG* disaccharide simulations were initiated with $\Phi = 266.0^\circ$, $\Psi = 38.9^\circ$ (Fig. 4). This conformation represents the structure reported in several empirical studies investigating natural alginate. Upon deprotonation, this conformation changes to the starting position $\Phi = 276.8^\circ$, $\Psi = 253.3^\circ$ (Fig. 4) due to the interaction of carboxylate groups, and represents the more likely in situ conformation

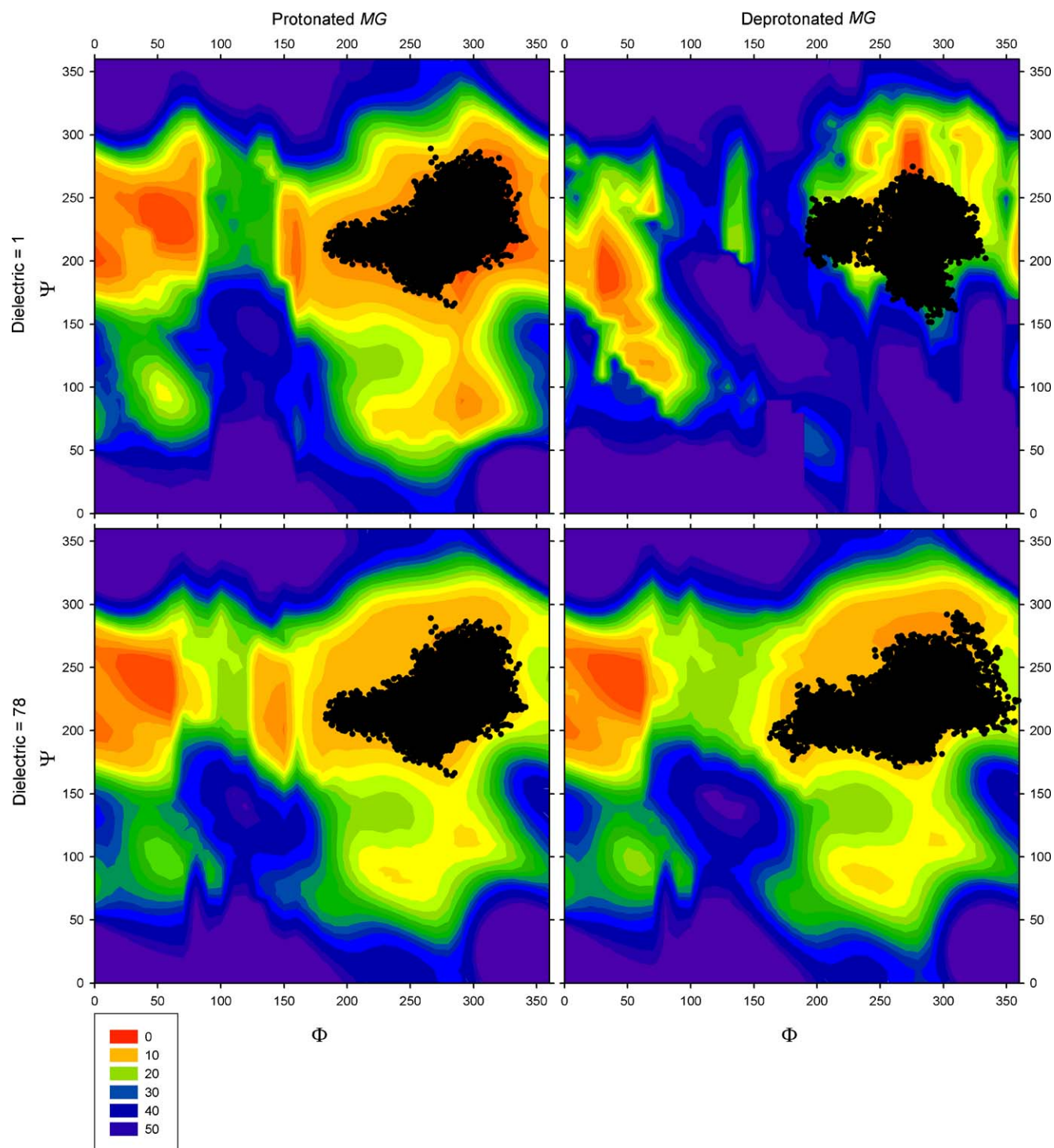


Fig. 5. Molecular dynamics simulation (100 ps) of the torsional changes of protonated and deprotonated mannuronic/guluronic disaccharides (*MG*) at 300 K superimposed over contour plots of the energy minima of the disaccharide. Contours are provided in kcal mol⁻¹.

because of the low pK_a of the carboxylate group. Deprotonated *GG* disaccharides exhibited a similar conformational preference associated with minimum *a* as observed for *MM* disaccharides (Fig. 4) and the disaccharides similarly explored energy troughs about their minimum energy conformations. It is significant to note that the protonated *GG* disaccharide did not have sufficient energy at 300 K to move from the local minimum *d* to the global minimum *a*.

MG disaccharide simulations began at $\Phi = 301.2^\circ$, $\Psi = 235.3^\circ$, and further demonstrate the stability of the preferred molecular arrangement associated with global minimum *a* (Fig. 5). The *MG* disaccharide exhibits movement to higher energy levels at 300 K than demonstrated by *MM* and *GG* disaccharides. These greater variations in torsion angle results from the increased thermal energy, and, therefore, least stable minima of *MG* disaccharides in

comparison with the *MM* or *GG* disaccharides (Table 4).

To demonstrate the effect of initial torsion angle configuration on disaccharide conformation, molecular dynamics simulations were also run with protonated *MM* and *GG* disaccharides, $\epsilon = 1$ (Fig. 6), but starting with a configuration corresponding to the local minimum *b* (*MM*: $\Phi = 50.0^\circ$, $\Psi = 243.0^\circ$; *GG*: $\Phi = 59.0^\circ$, $\Psi = 242.0^\circ$). The results show that both *MM* and *GG* disaccharides evolve from the local minimum *b* to the global minimum *a*, indicating that at 300 K there is an energetic preference for transition to the stable conformation at minimum *a*. The potential energy surface exhibits an increased breadth of the trough and relatively low energy barrier to ease the transition through this saddle point. Comparison of these dynamics results to those for the protonated *GG* (viz. Fig. 4) demonstrate that this barrier is lower than the energy barrier for conformational shift from minima *d* to *a*. Presumably, with enough thermal energy the molecule should be able to surpass this energy barrier and achieve conformation *a*.

To assess the significance of the energy barrier, simulations were performed at 400 K with the original starting configurations of *MM* and *GG* disaccharides (Fig. 7). Indeed, after occupying minimum *d*, the *GG* disaccharide proceeds to the configuration represented at minimum *a*. However, these simulations do not indicate any preference, temporary or otherwise, of the disaccharide for the local

minimum *b* conformation. In contrast, the additional thermal energy allows the *MM* disaccharide to move relatively freely between configurations represented by minima *a* and *b*, indicating that this barrier is lower for the *MM* disaccharide than for the *GG* disaccharide.

Based on the molecular dynamics simulation results represented in Figs. 3–7, the expected variation in the torsion linkages of alginic acid disaccharides is evaluated (Table 5). Independent of starting conformation, the preferred conformation of disaccharides is primarily associated with the global potential energy minimum *a*.

3.3. Molecular dynamics simulations with polymers

To extend the 2-unit models to polymers, alginic acid disaccharides *MM* and *GG* were repeated to form initial 20-unit polysaccharide models, configured with bond geometry corresponding to the simulated global energy minimum. Molecular dynamics simulations performed at 300 K provide trajectories for the equilibrated polymers that further reinforce the stability associated with the torsional geometry characterized by the potential energy trough at minimum *a* (Fig. 8). Some polymer linkages appear to access other minima regions and may be stabilized by intramolecular interactions throughout the polymer chain. Access of these other minima regions may represent the mechanism of stabilizing conformations associated

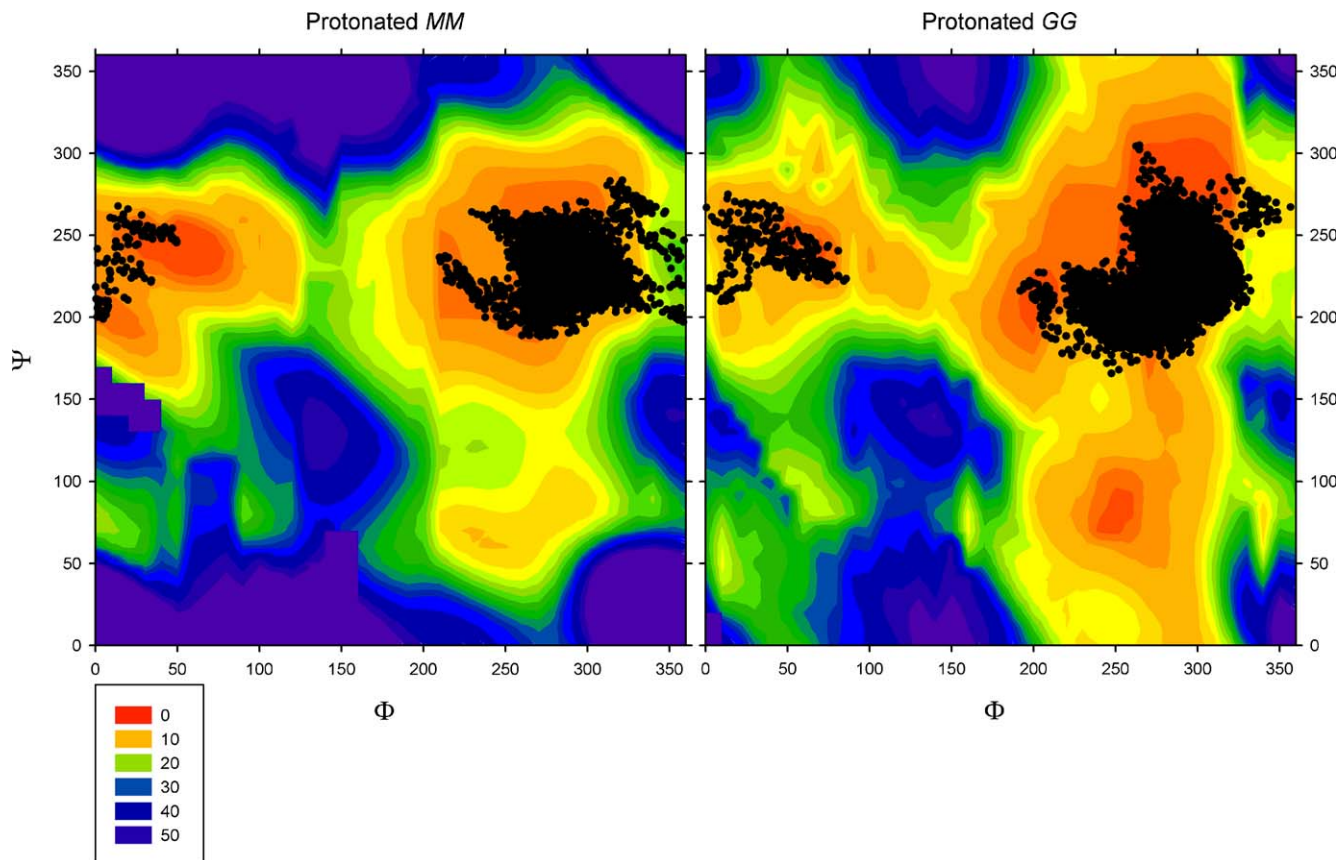


Fig. 6. Molecular dynamics simulation (100 ps) of protonated mannuronic and guluronic disaccharides started at the local minimum *b* at 300 K, $\epsilon = 1$. Contours are provided in kcal mol⁻¹.

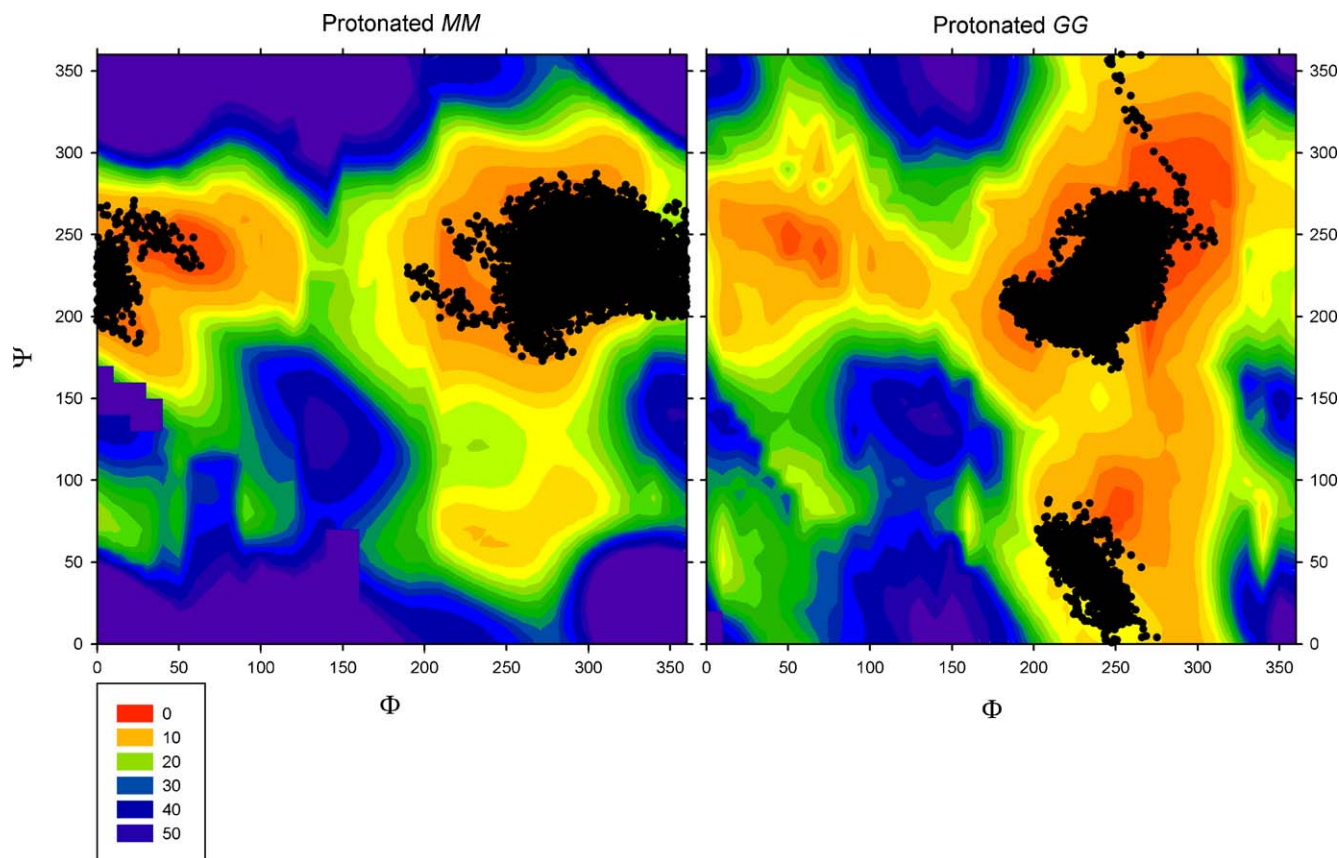


Fig. 7. Molecular dynamics simulation (100 ps) of protonated mannuronic (*MM*) and guluronic (*GG*) disaccharides at 400 K, $\epsilon = 1$, started at the local minima *b* and *d*, respectively. Contours are provided in kcal mol⁻¹.

Table 5
Torsional variation of protonated and deprotonated alginic acid disaccharides during dynamics simulation

Disaccharide	Φ (°)	Ψ (°)
Protonated <i>MM</i>		
$\epsilon = 1$	288.3 ± 16.3	227.7 ± 10.5
$\epsilon = 78$	274.5 ± 31.6	233.7 ± 17.3
Deprotonated <i>MM</i>		
$\epsilon = 1$	258.6 ± 30.7	227.1 ± 11.4
$\epsilon = 78$	274.5 ± 31.6	233.7 ± 17.3
Protonated <i>GG</i>		
$\epsilon = 1$	260.8 ± 9.5	44.8 ± 13.8
$\epsilon = 78$	257.5 ± 11.4	49.8 ± 12.6
$\epsilon = 1^a$	274.2 ± 19.6	225.0 ± 19.4
Deprotonated <i>GG</i>		
$\epsilon = 1$	266.3 ± 14.4	234.7 ± 19.1
$\epsilon = 78$	276.7 ± 17.1	222.8 ± 17.9
Protonated <i>MG</i>		
$\epsilon = 1$	278.5 ± 29.1	226.4 ± 20.0
$\epsilon = 78$	278.2 ± 29.0	226.1 ± 19.9
Deprotonated <i>MG</i>		
$\epsilon = 1$	276.4 ± 28.0	219.9 ± 20.4
$\epsilon = 78$	270.8 ± 35.0	221.9 ± 19.9
Average ^b	274.1 ± 7.2	227.2 ± 4.8

^a Simulation performed at 400 °K. Statistics performed after molecule stabilized at local minimum B (viz. Fig. 7).

^b Excludes protonated *GG* simulations conducted at 300 K.

with kinks or bends in the linear polymer chain. Temperature does not greatly affect the conformation of the polymers in terms of torsional access to the other minima regions (Fig. 9). In fact, increasing the temperature for simulations to 400 K appears to constrain the polymeric linkages around minimum *a*, although there is increased Φ - Ψ variation within the energy trough. This result may be due to the increase in intrapolymeric interactions that favor a straight-chain conformation. The only exception is a single linkage on the *G*-polymer, which may be the result of a significant bend in the polymer creating greater intramolecular nonbonded interactions.

3.4. Association of calcium ions with disaccharides and polymers

The previous simulations are necessary for developing a baseline understanding of the effects of structural conformation and configuration on the three-dimensional form of alginic acid subunits. However, these polysaccharides are likely associated with charged cations in situ. The cations act to stabilize otherwise unfavored conformations. To assess the relative stability of cation binding by different conformations and configurations of disaccharides, calcium ions were manually docked with the previously determined energy-minimized structures of deprotonated disaccharides and then subsequently energy-minimized

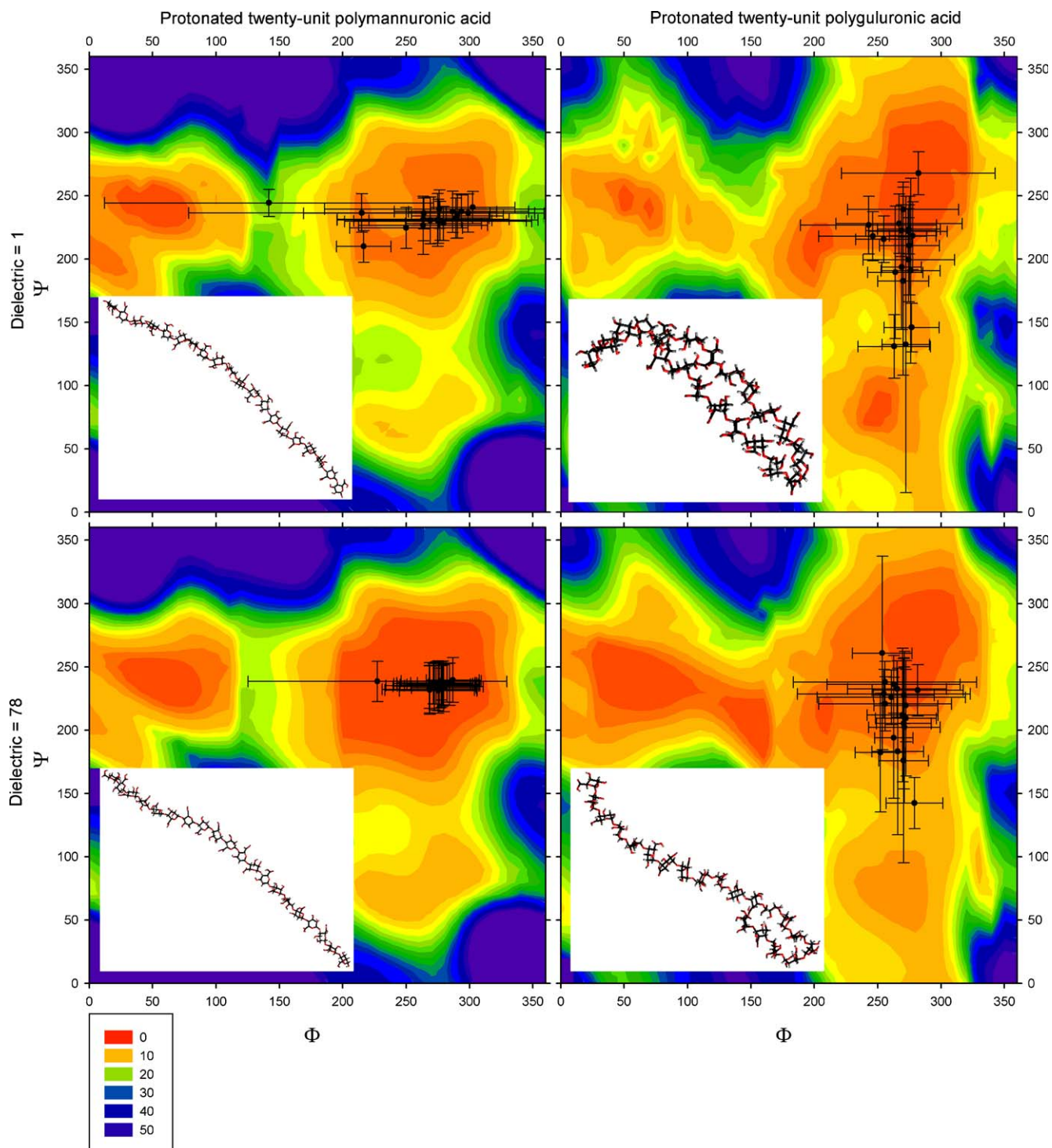


Fig. 8. Molecular dynamics simulation of 20-unit polysaccharides at 300 K. Each data point represents a single ether linkage and error bars represent one standard deviation in the torsional states experienced by that bond. The final configuration of the simulations is shown in the insets. Contours are provided in kcal mol⁻¹.

without any atomic or geometry constraints (Fig. 10). Electronic structure optimizations of the Ca²⁺-disaccharide complexes were also completed (see below). The proximity of oxygen electron-donating moieties to calcium during chelation by deprotonated alginic acid disaccharide units and the effect on torsion and relative stability are summarized in Table 6. E_{Total} was calculated as in Table 2 for

the entire simulation system including the calcium ion, and the binding energy (E_{Bind}) was calculated as follows:

$$E_{\text{Bind}} = E_{\text{Total}(\text{Ca}^{2+}\text{-dimer})} - E_{\text{Total}(\text{dimer})}. \quad (3)$$

The force field-based results indicate strong binding of the calcium ion by all the representative disaccharides. However, binding and complex stability vary, depending

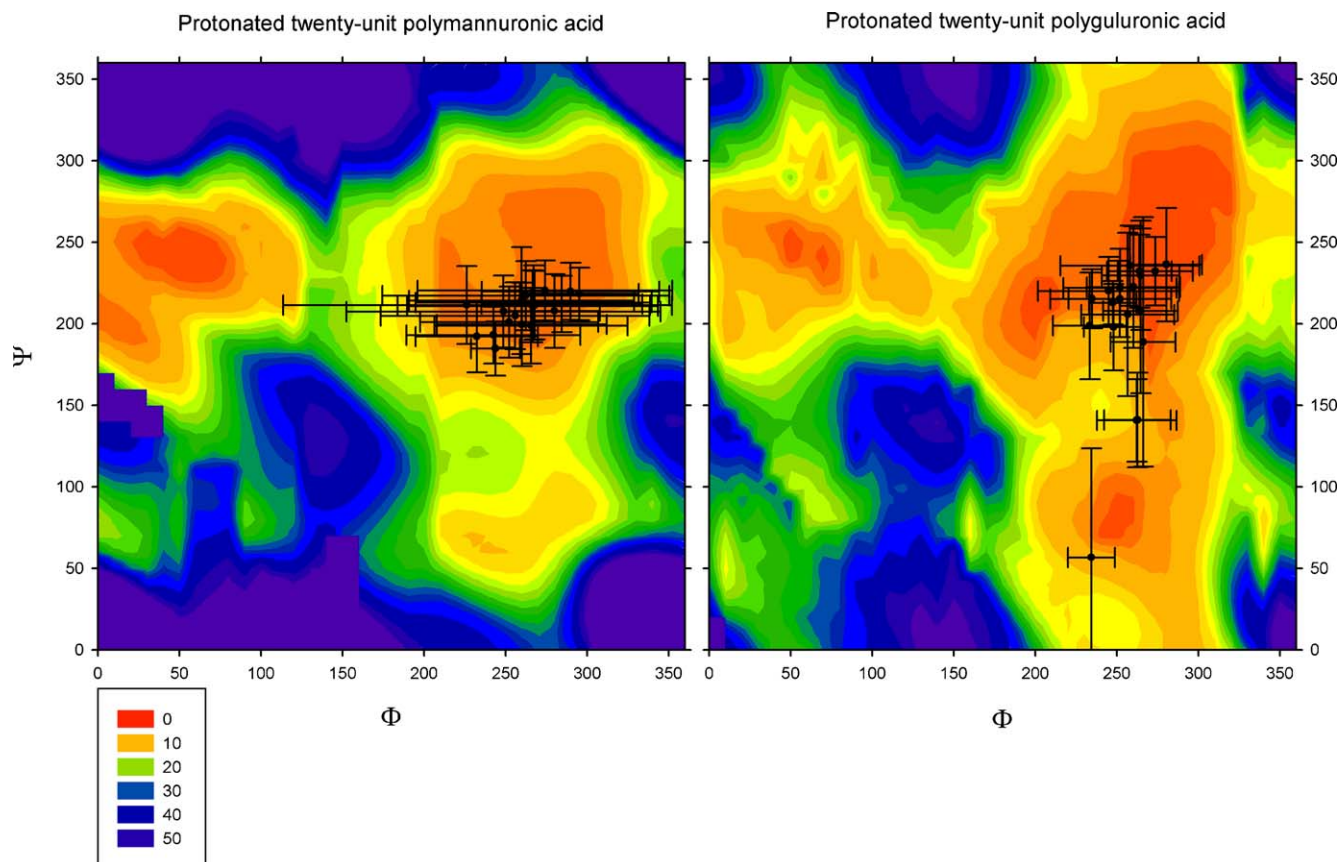


Fig. 9. Molecular dynamics simulation of 20-unit polysaccharides at 400 K and $\epsilon = 1$. Each data point represents a single ether linkage and error bars represent one standard deviation in the torsional states experiences by that bond. Contours are provided in kcal mol^{-1} .

on torsion angles, from the optimum values associated with minimum *a* in some cases (Braccini and Pérez, 2001). For example, the *MM* disaccharide appears to have the greatest stability when binding calcium in a conformation associated with the minimum *b* (Table 6, Fig. 10). The *GG* disaccharide has two stable conformations when associated with calcium near the minimum *a*. The conformations varied depending on the localization of the calcium with the disaccharide, i.e. placement near or far from the disaccharide-linkage ether (Emmerichs et al., 2004). Interestingly, near association with the disaccharide-linkage ether is a more energetically favorable state, presumably due to the closer association with stabilizing oxygens. Additionally, the *GG* disaccharide will not maintain a conformation corresponding to minimum *b* and instead favors a conformation reminiscent of minimum *d* in simulations at $\epsilon = 1$ with protonated *GG*. *MG* disaccharides exhibit stable conformations associated with minima *a* and *b*. When associated with calcium, these disaccharides also are stable in a conformation reminiscent of minimum *c* in simulations at $\epsilon = 1$ with protonated *GG*, indicating the α -linkage of this disaccharide may play a significant role in development of stable cation complexes (Lattner et al., 2003). The Coulombic energy stabilization gained by the formation of a relatively strong Ca^{2+} -carboxylate coordination in all

disaccharides easily offsets the destabilization introduced by transients in the Φ - Ψ angles. The exact energy gain also needs to include the hydration energy of a calcium ion in solution, and any destabilization associated with coordinated water molecules at the binding site. Overall, the disaccharides exhibit relatively high binding energies with Ca^{2+} , and demonstrate the efficient coordination and strength of the carboxylate groups and other oxygen moieties at the binding site.

Energy-optimized electronic structure configurations for the Ca^{2+} -*MM-a*, Ca^{2+} -*GG-a*, and Ca^{2+} -*MG-a* disaccharides were derived for comparison to the force field results. As was observed for the protonated and deprotonated systems, there is excellent agreement in the results derived from the two methods. Comparisons of bond distances, bond angles, and torsion angles are similar to those noted previously for the neutral molecules and anions. Mean Ca–O distances associated with the metal complex are slightly extended for the quantum results (2.36 Å versus 2.34 Å observed for the force field method). One exception to this favorable comparison is that the force field simulation of the Ca^{2+} -*MM-a* disaccharide failed to reproduce the triple coordination of the carboxylate oxygens to the Ca^{2+} that was observed in the electronic structure optimization; both carboxylate oxygens from each of the two carboxylate

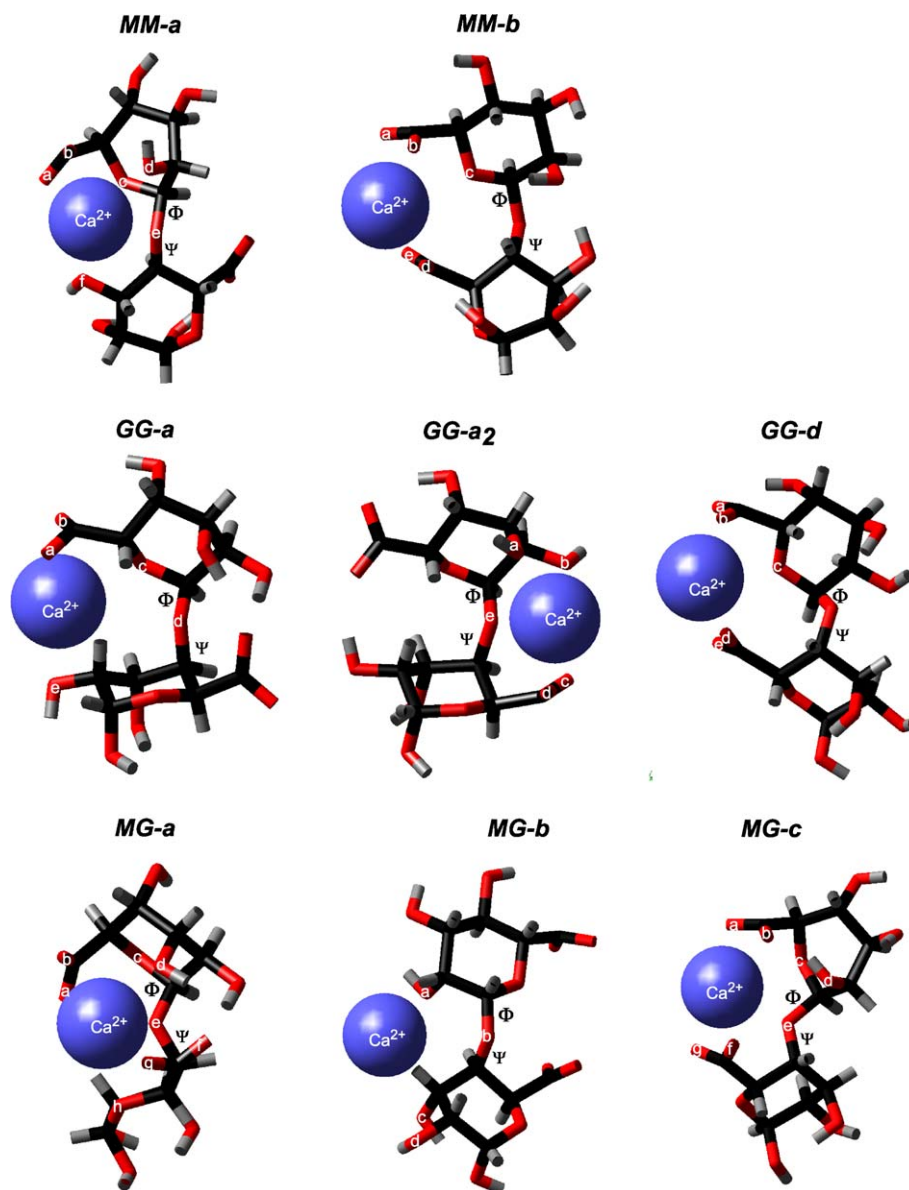


Fig. 10. Energy-minimized structures of alginic acid subunit disaccharides associated with calcium ions. Data for oxygen–calcium distance, bond torsion, and binding and total energies are presented in Table 6. Color key: black = carbon, red = oxygen, gray = hydrogen, blue = calcium.

Table 6

Proximity of oxygen electron-donating moieties to calcium during chelation by deprotonated alginic acid disaccharide units and the effect on torsion and relative stability

Distance to Ca^{2+} (Å)	<i>MM-a</i>	<i>MM-b</i>	<i>GG-a</i>	<i>GG-a₂</i>	<i>GG-d</i>	<i>MG-a</i>	<i>MG-b</i>	<i>MG-c</i>
<i>a</i>	2.39	2.35	2.39	2.39	2.36	2.34	2.95	2.31
<i>b</i>	2.36	2.34	2.32	2.42	2.44	3.34	3.43	2.34
<i>c</i>	2.65	3.00	2.84	2.60	2.58	3.84	3.52	3.55
<i>d</i>	2.66	2.29	3.77	2.30	2.28	2.50	3.72	3.67
<i>e</i>	2.35	2.80	2.56	3.38	2.30	2.51	—	2.79
<i>f</i>	2.42	—	—	—	—	3.30	—	2.34
<i>g</i>	—	—	—	—	—	2.27	—	2.30
<i>h</i>	—	—	—	—	—	2.63	—	—
Φ (°)	282.3	44.8	247.1	275.1	267.4	212.3	69.7	187.1
Ψ (°)	258.6	246.7	204.2	192.5	13.5	209.6	236.5	174.8
E_{Bind} (kcal mol ⁻¹)	-412.60	n.d.	-367.64	-403.68	n.d.	-499.64	n.d.	n.d.
E_{Total} (kcal mol ⁻¹)	-338.86	-412.80	-303.30	-339.35	-410.10	-423.61	-416.64	-412.67

n.d. = not determined.

groups bind equally to the Ca^{2+} in the force field results. Nonetheless, binding energies for the Ca^{2+} derived from the two approaches are in fairly good agreement: $-489.4 \text{ kcal mol}^{-1}$ versus $-412.6 \text{ kcal mol}^{-1}$ for Ca^{2+} -*MM-a*; -443.9 versus $-367.6 \text{ kcal mol}^{-1}$ for Ca^{2+} -*GG-a*; -522.3 versus $-499.6 \text{ kcal mol}^{-1}$ for Ca^{2+} -*MG-a*. Although the energy values exhibit up to 20% relative differences (which is quite good for force field methods), the comparison shows a consistency in the relative binding energy for the complexes with the *MG* disaccharide being the most efficient in binding to the cation. The calculated binding energies are more stabilizing than the $-381 \text{ kcal mol}^{-1}$ enthalpy observed for hydration of Ca^{2+} (Rosseinsky, 1965), although no water molecules were incorporated in the models, which would effectively reduce the strength of the binding of the disaccharide to the Ca^{2+} .

To assess polymer binding of cations, energy-minimized disaccharides associated with calcium ions were used to construct polymer models, which were subsequently energy minimized using the atom-based force field method (Fig. 11). It would be computationally expensive to complete electronic structure calculations for these larger systems. The binding energies of the polymer-calcium complexes per calcium ion are (kcal mol^{-1}): *MM-a* = -344.2 , *MM-b* = -350.5 , *GG-a* = -324.0 , *GG-a₂* = -314.1 , *GG-d* = -361.0 , *MG-a* = -351.0 , *MG-b* = -322.8 , with the *GG-d* exhibiting the most stable configuration. The 20-unit polysaccharides exhibit reduced binding per calcium than

the disaccharides (viz. Table 6) because intermolecular interactions and steric hindrances along the polysaccharide chain limit the efficiency of the calcium binding. *MM* and *MG* polymers were significantly less buckled than *GG* polymers. All polymers were stabilized by Coulombic interactions, which allowed for increased bond strain (e.g. *MG-a*). Further stabilization of the polymers is expected with the addition of extra polymer chains to form polymeric bundles and extended two-dimensional structures. However, these complex structures are beyond the present scope of the investigation and will need to be addressed in a future study.

The conformation and configuration of alginic acid disaccharides have been shown to be important in molecular energy stability, with a similar global energy minimum conformation for all representative subunits. These conformations are favored in polymers, as well, but intramolecular stabilization allows limited exploration of less-favored conformations. The simulations demonstrate that Coulombic stabilization by cations is a determining factor for disaccharides to stabilize at other conformations than those determined by bonded energy terms. Torsional states experienced by disaccharides associated with calcium are significantly different from the global energy minimum. The greater stabilization effect is apparent when modeling cations with polymers where cations can be observed interacting with several monosaccharides (Fig. 11).

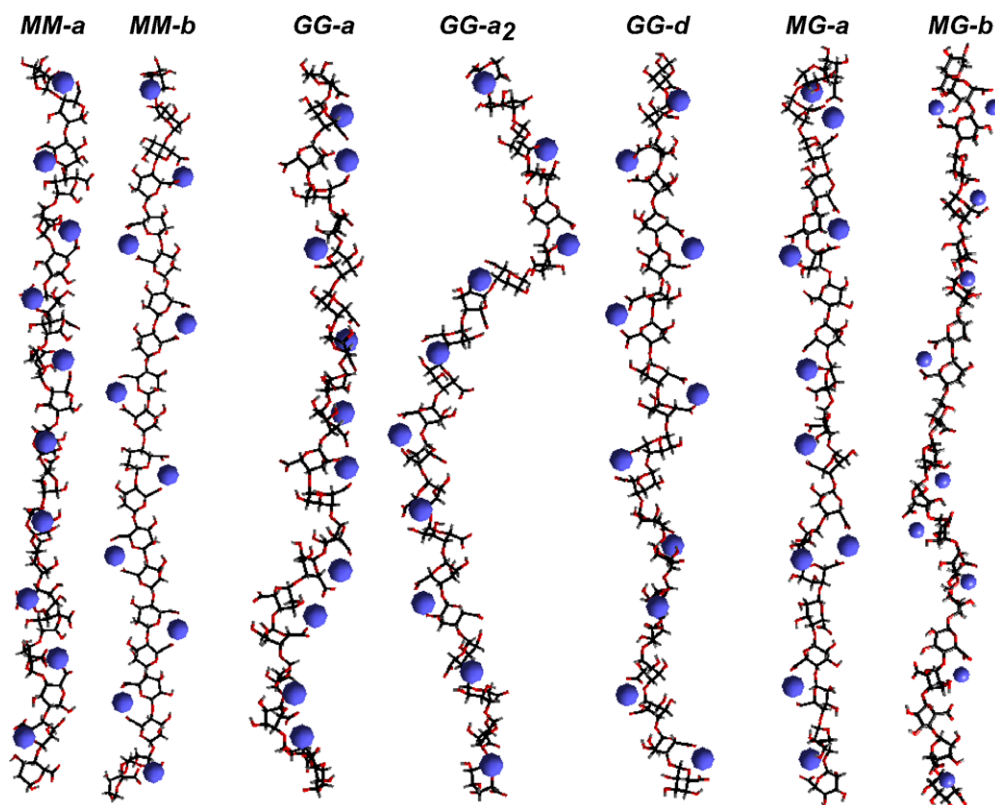


Fig. 11. Energy-minimized structures of polymers in different torsional conformations corresponding to different starting positions of torsional energy minima associated with calcium ions localized in potential chelation sites. Color key: black = carbon, red = oxygen, gray = hydrogen, blue = calcium.

3.5. Simulations with alginic acid disaccharides and the (10 $\bar{1}$ 4) calcite face

Molecular dynamics simulations were performed to determine the role of conformation of alginic acid subunits on sorption to the (10 $\bar{1}$ 4) calcite surface. The disaccharides are initially positioned in the simulation cell and allowed to interact with the surface and in solution in two conformations: the global energy minimum (*a*) and a local energy minimum (*b*), as previously determined. The disaccharides are compared as aqueous species and surface-sorbed complexes (viz. Fig. 2). The most stable orientation and binding distance to the calcite surface for each disaccharide were systematically determined before performing the MD simulations. The sorption energy is determined by taking the difference of the potential energy of the simulation cells Eq. (1) for the two different positions of the disaccharide within the simulation cell. This approach provides a convenient alternative for evaluating the sorption enthalpy since the simulation cells are identical except for the placement of the molecule. Hence, any differences in the energy values are the result of the disac-

Table 7
Torsional variation of the ether linkage during 50 ps molecular dynamics simulations for solvated and sorbed (calcite (10 $\bar{1}$ 4) surface) disaccharides

Disaccharide	$\Phi \pm$ Standard deviation ($^\circ$)	$\Psi \pm$ Standard deviation ($^\circ$)
<i>GG</i>		
<i>a</i> Starting conformation: ^a		
$\Phi \sim 256, \Psi \sim 233$		
Solvated	223.4 \pm 10.5	216.3 \pm 7.4
Surficial	274.5 \pm 8.0	274.0 \pm 6.6
<i>b</i> Starting conformation: ^b		
$\Phi \sim 61, \Psi \sim 284$		
Solvated ^c	280.0 \pm 18.9	258.3 \pm 24.0
Surficial	51.0 \pm 7.1	269.8 \pm 7.2
<i>MG</i>		
<i>a</i> Starting conformation: ^a		
$\Phi \sim 290, \Psi \sim 231$		
Solvated	268.0 \pm 9.5	206.4 \pm 14.0
Surficial	280.6 \pm 9.8	271.3 \pm 6.7
<i>b</i> Starting conformation: ^b		
$\Phi \sim 70, \Psi \sim 230$		
Solvated ^c	201.3 \pm 9.4	220.3 \pm 9.3
Surficial	36.0 \pm 6.9	238.8 \pm 6.0
<i>MM</i>		
<i>a</i> Starting conformation: ^a		
$\Phi \sim 197, \Psi \sim 221$		
Solvated	196.0 \pm 11.6	221.9 \pm 10.6
Surficial	262.1 \pm 8.5	214.4 \pm 7.2
<i>b</i> Starting conformation: ^b		
$\Phi \sim 52, \Psi \sim 225$		
Solvated ^c	277.5 \pm 15.3	229.7 \pm 12.5
Surficial	218.6 ^d	193.0 ^d

^a *a*, Global energy minimum.

^b *b*, Local energy minimum.

^c During equilibration (initial 20 ps) these simulations have shifted to the global energy minimum (*a*) conformation (viz. Fig. 15).

^d Torsional values are the final values recorded from the 20 ps equilibration simulation (due to instabilities in the production simulation).

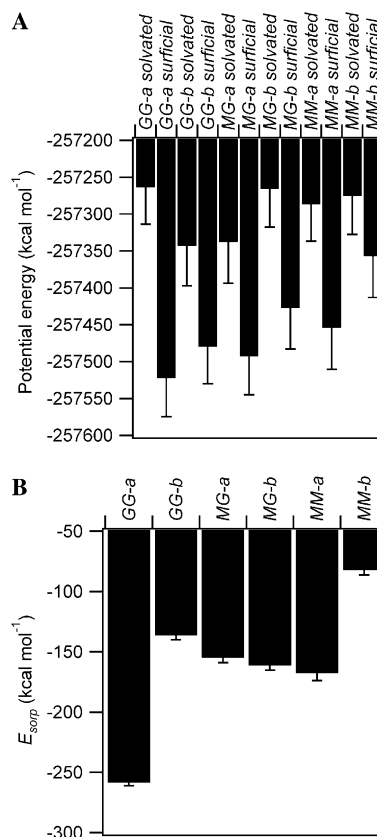


Fig. 12. Average potential energy (\pm standard deviation) of the simulation cells (A) and the disaccharide sorption energy (B) derived from the 50 ps production simulations. *MM-b* data is recorded from the 20 ps equilibration run due to instabilities in the 50 ps production run.

charide interactions with the solvating water molecules and with the calcite surface. However, it is important to note that the energy determinations are useful for relative comparison of the systems but should not be considered comparable to absolute or in situ energies. Molecular dynamics simulations were conducted and analyzed for all the representative disaccharides. The results are provided in Table 7 and Fig. 12. As noted previously, only a detailed account of the relevant chemistry for the *GG* disaccharide is presented; similar phenomena to those described in the following sections control the energetics of the other disaccharides.

The surface-sorbed (surficial) configuration for each of the disaccharides is found to be the more stable (Fig. 12A) of the two simulations and sorption is exothermic (de Leeuw and Cooper, 2004). The solvated forms of the disaccharides all exhibit a higher potential energy because of, in part, the charged carboxylate groups. Interaction of the disaccharides with the surface allows localization of the negatively charged carboxylates and the positively charged calcium ions at the mineral surface. The sorption energies of the disaccharides were calculated to compare the magnitude of the interaction of the different disaccharides with the calcite surface (Fig. 12B). The disaccharide-conformation of *GG-a* is significantly more stable on the calcite surface and is stabilized by approximately

250 kcal mol⁻¹. The *GG* disaccharide has been experimentally demonstrated to form stronger interactions with aqueous cations due to the appropriate spacing and configuration of cation-stabilizing moieties. It is likely that the same features allow the disaccharide to strongly interact with the cations on the calcite surface. The *MG-a* and *-b* disaccharides also formed stable associations with the calcite surface. Although *GG*-blocks have consistently been reported as the chelating portion of alginic acid, *MG*-blocks have recently been implicated as being able to bind aqueous cations (Lattner et al., 2003).

The differences in the sorption energies of the *GG-a* and *GG-b* disaccharides indicate that there is significant conformational control of disaccharide interaction by the calcite (10 $\bar{1}$ 4) surface. These two disaccharides are chemically identical and differ only in their starting torsional arrangements. The role of conformation on localization of the active sorption moieties of the disaccharides was compared for the *a* and *b* conformations of *GG*.

The conformations of the *GG* disaccharides control interaction of the electron-donating moieties with the cations of the surface (Fig. 13) (Emmerichs et al., 2004). Contour plots of the density of the actively binding atoms derived from the trajectories demonstrate that the *GG-a* disaccharide interacts with the surface with one carboxylate group, two ether oxygens, and several hydroxyls. The *GG-b* disaccharide interacts with a single carboxylate, a single ether oxygen, and multiple hydroxyls. An important difference in the two arrangements is the disposition of the ether oxygen associated with the ring linkage (>C–O–C<). In the *GG-a* form, the ether oxygen linking the monosaccharides is in close proximity to the calcite surface, whereas in the *GG-b* form the ether oxygen is situated up and away from the surface. The additional stabilization provided by the interaction of this relatively immobile ether oxygen, in comparison to hydroxyls, appears to substantially affect the sorption energy.

The relative importance of the various electron-donating portions of the disaccharides is quantified by measuring the radial distribution functions (RDF) for Ca–O interactions, specifically for the oxygen atoms in the disaccharides and the calcium atoms in the first surface layer of the calcite (Fig. 14). The ether oxygens on the *GG-a* disaccharide interact most strongly with the calcite surface as characterized by the dominant RDF peak at 3.6 Å, whereas for the *GG-b* disaccharide the equivalent RDF is significantly diminished. On the *GG-b* disaccharide, the hydroxyls appear to be the dominant interacting moieties as indicated by the main peak that is centered at 3.7 Å. However, the relative freedom of these atoms in comparison to the ether oxygens results in a less controlled association, as evidenced by the substantial breadth of this Ca–O RDF peak.

Simulations having the disaccharides initially in the local potential energy conformation (*b*) all reverted to the global energy minimum (*a*) during the equilibration simulations. The solvated *GG-b* disaccharide quickly (within several picoseconds) transformed into the global energy

minimum (*a*) conformation during the preproduction equilibration simulation (Fig. 15). An analysis of the variation in the two torsion angles (Ψ and Φ) associated with the disaccharide ether linkage provides a good metric for this transformation. It appears that at 0.1–0.9 ps, the torsion angle Ψ varies to allow rotation of torsion angle Φ about the –C–O– bond, after which both torsion angles reequilibrate to the stable conformation associated with the global energy minimum (*a*). The coordinated rotations result in a potential energy stabilization of approximately 300 kcal mol⁻¹. Closer inspection of the torsion angles reveals that each variation in one of the torsion angles results in complementary opposing changes of the other, so as to reduce the steric hindrance of the remaining disaccharide structure and avoid destabilization.

While this study has expanded on the interactions of the *GG* disaccharide, similar analyses were conducted with *MM* and *MG* disaccharides (viz. Table 7 and Fig. 12). A similar movement from the local energy conformation (*b*) to the global potential energy minimum (*a*) conformation is observed for all disaccharides when solvated (Table 7). The potential energy barrier for movement from the *b* to the *a* conformation is relatively low (<20 kcal mol⁻¹) and the transition has been shown to readily occur at 300 K for *GG* and *MM*.

MM-b is the only disaccharide to revert from the *b* conformation to the *a* conformation when associated with the calcite surface (Table 7). For other disaccharides, interaction with the calcite surface maintained the local energy minima conformation (Table 7) and the stabilization was the result of interactions of the disaccharide with surface cations (viz. Figs. 13 and 14). The *MM-b* disaccharide has the lowest E_{sorp} with the calcite surface (viz. Fig. 12) due to the β -linkage of the disaccharide and resultant equatorial orientation of the electron-donating and charged oxygens on the disaccharide. The strong Coulombic interactions of the carboxylate groups and their orientation due to the α -linkages of the *GG* and *MG* disaccharides control their torsional rotation when associated with the calcite surface. Conversely, the more planar nature of the β -linkage on the *MM* disaccharide allows a less energetically constrained rotation and fewer close-range repulsions with the calcite surface.

The presence of disaccharides disrupts hydration of the calcite surface (Fig. 16). When the disaccharide is solvated in the bulk solution, water molecules are coordinately arranged on the calcite surface (Geissbühler et al., 2004; Kerisit and Parker, 2004b). Water molecules can be associated with a single surface cation (Fa et al., 2005; Stockelmann and Hentschke, 1999) or can interact with two cations, and additionally be stabilized by forming hydrogen bonds with the surface carbonate species. The doubly associated surface water molecules are aligned with the *y*-axis of our simulation cells because the carbonate species on the (10 $\bar{1}$ 4) calcite surface project out of the cleavage plane (viz. Fig. 13). Previous

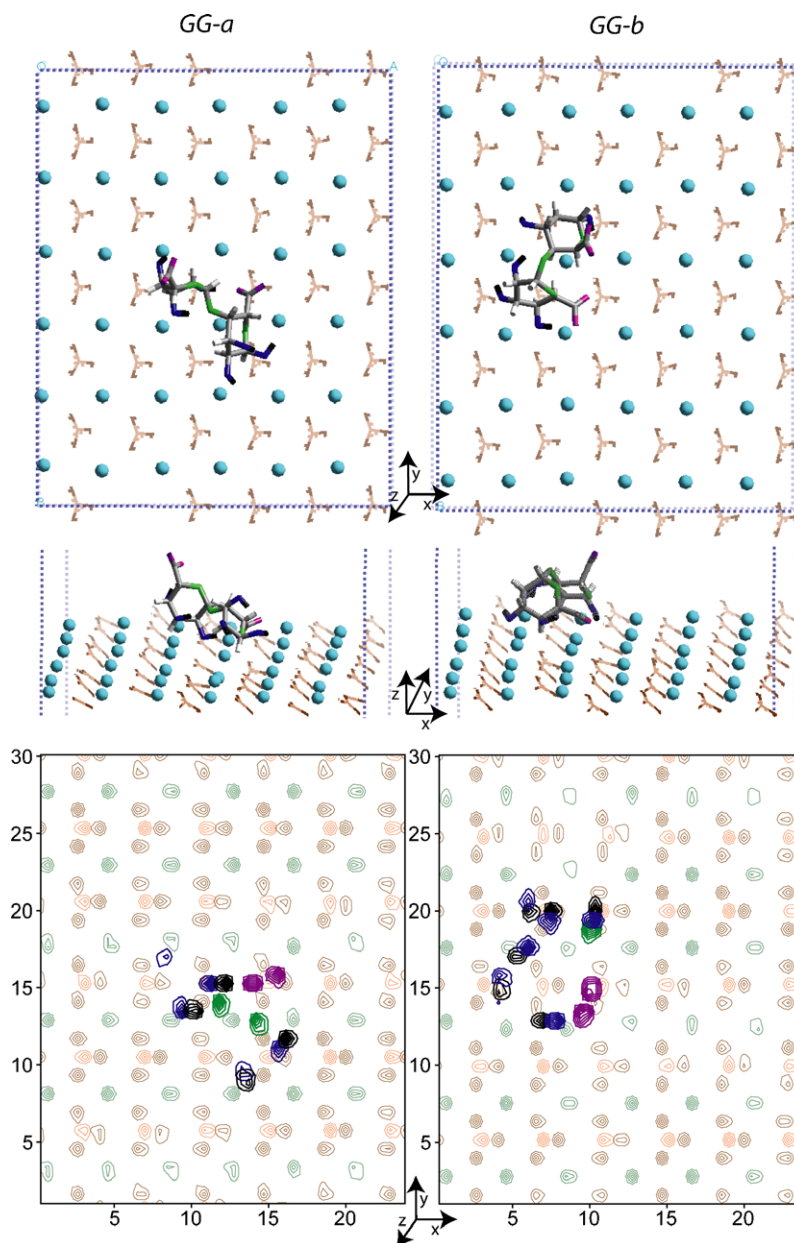


Fig. 13. Results of molecular dynamics simulations (50 ps) of the *GG* alginic acid disaccharide started from the global potential energy minimum (*a*) conformation (left) and a local potential energy minimum (*b*) conformation (right) on the $(10\bar{1}4)$ calcite surface with explicit hydration. Water molecules have been removed for clarity. A representation of the disaccharides and calcite surface are apparent from a plan view in the upper frames and a side view in the middle frames. The bottom frames provide the atomic density contours of the disaccharide and calcite atoms derived from atomic trajectories for the course of the production simulation. All plot axes are distances (\AA) and represent the dimensions of the simulation cell. Atoms are color coded as follows for calcite–calcium (light blue), calcite carbon (light brown), calcite oxygen (dark brown)—and for the disaccharide–carboxylate oxygen (purple), ether oxygen (green), hydroxyl oxygen (dark blue), hydroxyl hydrogen (black).

reports have found that hydration of the surface occurs similarly to our results of single coordination (de Leeuw and Parker, 1997). However, the previous studies have modeled only a single monolayer of water on the calcite surface. As noted above, surface hydration will be further stabilized by additional layers of water and the formation of a hydrogen bonded network.

Disaccharides associated with the calcite surface affect calcite hydration (Fig. 16). Association of the disaccharides causes displacement of water molecules from the

surface and a reduction in the hydration. Relative to other organic complexes (de Leeuw et al., 1998), the greater binding energy observed for alginic acid disaccharides on calcite has a greater influence on water displacement and surface hydration. Additionally, it appears that the presence of the sorbed disaccharides induces ordering of the water molecules on the calcite surface. The observed increase in the double-coordination of water to calcium when the disaccharide is surface-associated may be the result of the absence of

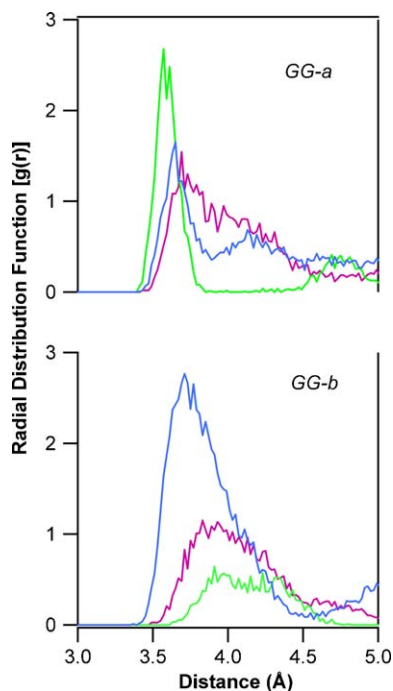


Fig. 14. Radial distribution functions for the disaccharide oxygen species and the calcium atoms in the first layer of calcite for the 50 ps simulation period. Hydroxyl (blue), carboxyl (red), and ether (green) oxygen species are colored similar to the representations in Fig. 13.

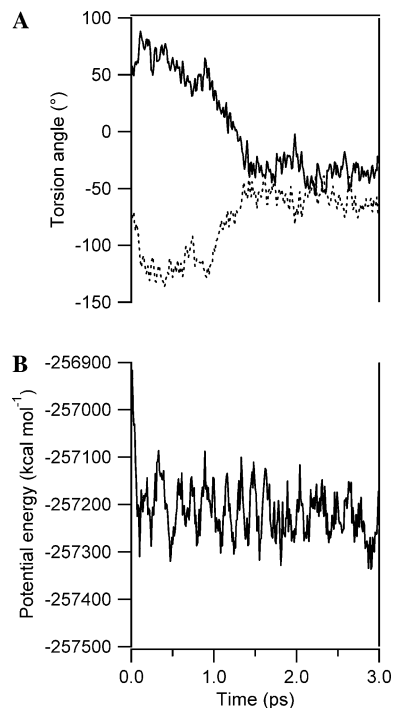


Fig. 15. Variation in torsion angles (solid line, Φ ; dashed line, Ψ) (A) and potential energy (B) of the solvated *GG-b* disaccharide during the initial 3 ps of the equilibration run.

disruptive long-range forces in comparison to when the disaccharide is solvated in the bulk solution. The conformation of the disaccharide affects the shape and

region of disrupted hydration. If the proper geometry is present, a disaccharide on the surface also appears to be able to further stabilize hydration. The water molecule associated with the ether linkage of the *GG-a* disaccharide is associated with both the calcite calcium below and by hydrogen bonding to the disaccharide above. These coordinations result in an ordered and stabilized disaccharide with both water and surface species, as demonstrated by the dense array of contour lines for the atomic densities in Fig. 13. Finally, Ca^{2+} -disaccharide complexes can occur at or near the surface either by association with aqueous species or by direct surface chelation (Perry et al., 2004). The reactivity of the calcite surface will be affected by the occurrence of these precipitated complexes.

3.6. Alginic acid binding at a surface defect on the calcite surface

Calcite dissolution by a microbially produced polysaccharide has been observed to occur via a crystallographically specific mechanism (Perry et al., 2004). Alginic acid has been observed to preferentially attack the obtuse steps of dissolution pits on the $(10\bar{1}4)$ calcite surface. We have begun to model the interactions of disaccharides at dissolution pits to understand their preferential attachment on the obtuse pit step. Previous work by us has hypothesized that imposed steric hindrance by the acute step limits the ability of alginic acid binding groups to form surface-active complexes and thereby limits ligand-promoted dissolution (Perry et al., 2004).

The energy landscape of a *GG-a* disaccharide about a dissolution pit was explored (Fig. 17). The dissolution pit was created by manual removal of a monolayer of surface atoms from the $(10\bar{1}4)$ calcite surface. Molecular dynamics simulations were not conducted due to energy instabilities associated with the pit edges, most likely due to pit-pit interactions across cell boundaries in the periodic systems. Fortunately, the force field can accommodate static energy calculations for organics with these highly defective surface topologies. The *GG-a* disaccharide was systematically moved around the different vertices of the pit and energy minimization allowed an exploration of the disaccharide preference for different regions of the pit.

The *GG-a* disaccharide preferred coordination with the *oo* and *aa* vertices of the carbonate pit, as opposed to the *oa* and *ao* (Fig. 17). Assuming that the relative impact of the surface of the pit bottom on disaccharide potential energy is the same at all four vertices, the destabilizing effect at any vertex must be the result of interactions with the pit edge. The *oo* and *aa* pit vertices terminate with a carbonate leaving two calcium ions relatively exposed. Conversely, the *oa* and *ao* vertices terminate with a calcium ion exposing two carbonates. The interactions of the disaccharide carboxylates with the calcite carbonates at these vertices likely control the

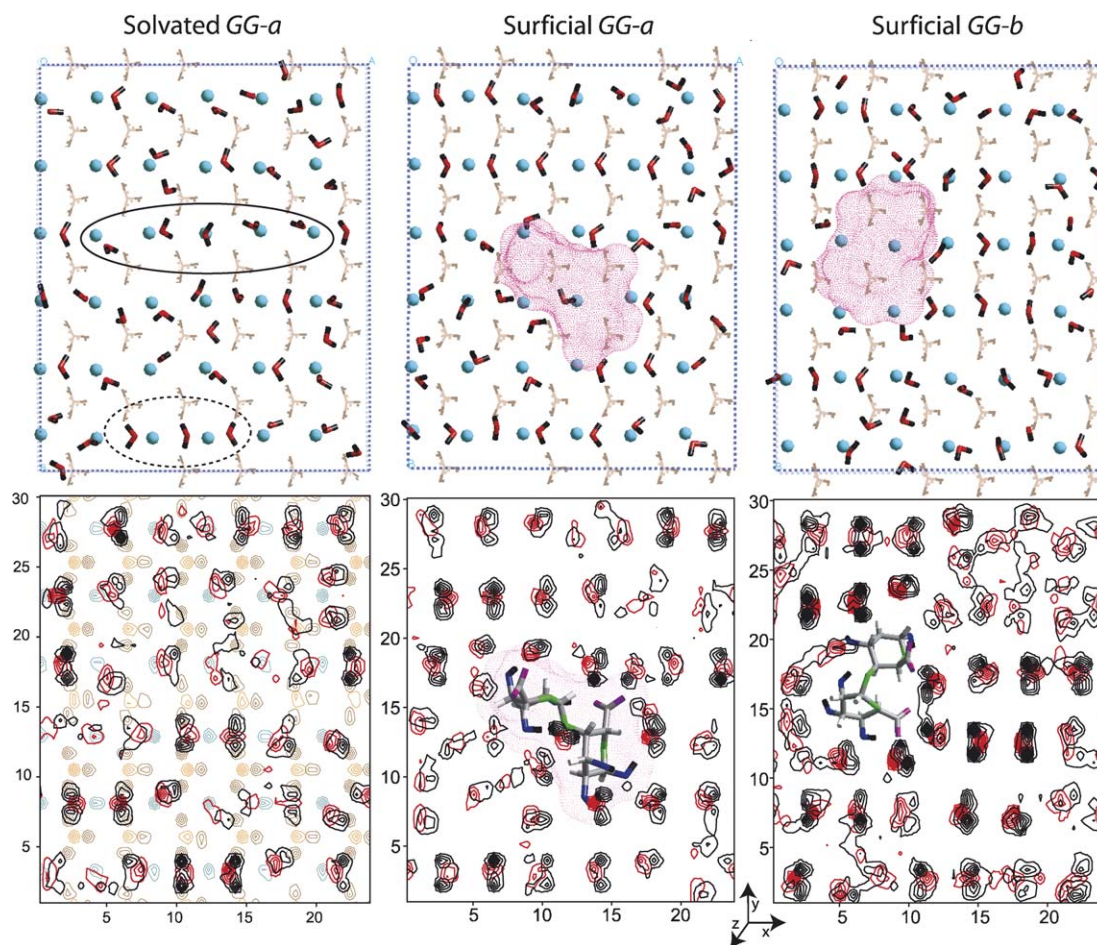


Fig. 16. Molecular dynamics simulation (50 ps) of the *GG* alginic acid disaccharide solvated (left), and in the global (*a*; middle) and local (*b*; right) potential energy minimum conformations associated with the (1014) calcite surface with explicit hydration. The top frames show the positions and conformations of the atoms near the calcite surface at 50 ps of the simulation. The bottom frames show the atomic density of the water and calcite atoms over the course of the simulation. Representations of the disaccharides with calculated Connolly surfaces and are superimposed to show the positions of the disaccharides. Water molecules interacting with single (solid line oval) and double (dashed line oval) surface cations are highlighted. All plot axes are distances (Å) and represent the dimensions of the simulation cell.

observed instabilities. The disaccharide was more stable by 6 kcal mol^{-1} at the *oo* versus the *aa* vertex. An extended study of the association of the major disaccharides conformations with calcite pits and pit edges would necessarily be conducted with larger simulation cells and long-duration molecular dynamics simulations.

4. Conclusions

Atomistic-scale predictive modeling is well suited for the evaluation of organic-inorganic binding reactions, especially those associated with the polysaccharide-based exudates nominally represented by alginic acid. In this study, the effects of ether-linkage torsion, intramolecular interactions, cation binding, and temperature on the conformation and relative stabilities of different representative disaccharide and polysaccharides were evaluated. Based on the molecular dynamics simulation results represented in Figs. 3–7, the expected variation in the torsion linkages of alginic acid disaccharides was

evaluated (Table 5). We determine that, independent of starting conformation, the preferred conformation of disaccharides is primarily associated with the global potential energy minimum *a*. This assertion is extended to most in situ environments, including marine and terrestrial locations, due to the effect of deprotonation and temperature on driving the disaccharides to this minimum conformation. Most alginic acid in situ are expected to be deprotonated at the carboxylate functionalities due to their relatively low $\text{p}K_a$ values. Torsional modification and molecular dynamics simulations indicate that deprotonated carboxylic groups on *MM*, *GG*, and *MG* disaccharides lead to an energetically favored conformation for all disaccharides at $\Phi = 274.1 \pm 7.2^\circ$, $\Psi = 227.2 \pm 4.8^\circ$. Intramolecular interactions within polymer chains stabilized some of the less-favored conformations. However, simulations of cation association with the disaccharides and polymers resulted in Coulombic interactions that greatly stabilized conformations removed from the global energy minimum. Calcium

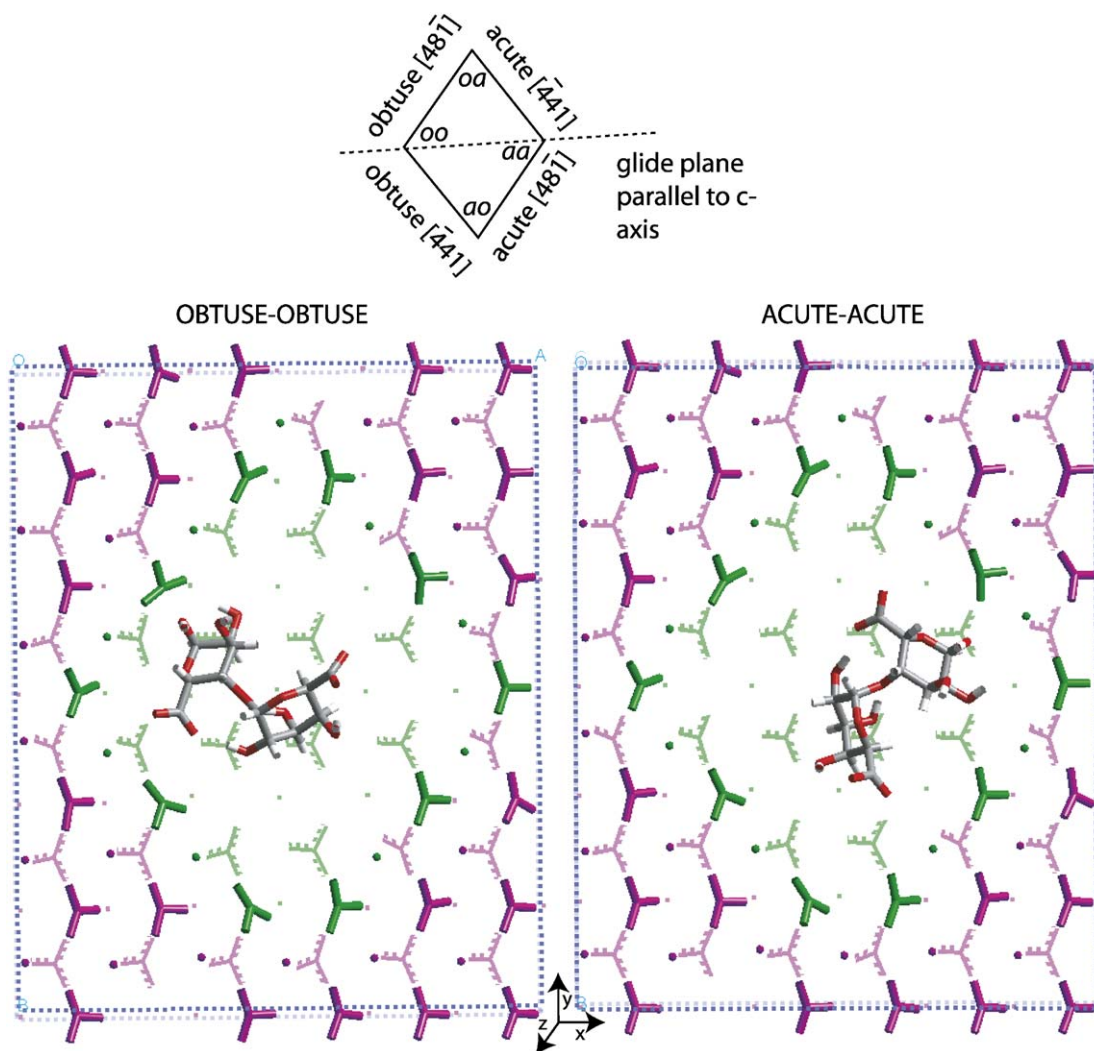


Fig. 17. Top-down view of the energy-minimized conformations of *GG-a* disaccharides associated with the *oo* and *aa* edges of a dissolution pit in the $(10\bar{1}4)$ calcite surface. Top calcite plane is represented by cylindrical bonds while the second calcite plane is denoted by stick bonds. The pit is highlighted by green coloration. Disaccharide color key: red, oxygen; gray, carbon; and white, hydrogen.

binding energies with the *MG* disaccharide and polymer indicate that these alternating monosaccharide blocks may have an underestimated role in cation binding in comparison to *MM* and *GG* alginate blocks (Lattner et al., 2003; Emmerichs et al., 2004). A hybrid energy force field for modeling interactions of organic molecules with carbonate mineral surface in hydrated environments was developed. This force field was used to investigate the interaction of alginic acid with the $(10\bar{1}4)$ calcite surface. Alginic acid disaccharides have a preferred conformation when solvated but have the ability to maintain other forms when associated with the calcite surface. The *GG-a* disaccharide forms the most stable complexes with the calcite surface. The differences in the binding energies of the different disaccharides are controlled by the proximity of electron-donating oxygen moieties on the disaccharides to cations on the calcite surface. The binding of organics to the calcite surface affects the amount and ordering of surface hydration. The

force field can also be applied to simulation of mineral surfaces with defects.

Acknowledgments

This work was supported in part by a Sandia National Laboratories Campus Executive Fellowship to T.D.P., R.T.C. acknowledges the support provided by the Chemical Sciences, Geosciences, and Biosciences Division of the Office of Basic Energy Sciences in the U.S. Department of Energy. Sandia is a multiprogram laboratory operated by Sandia Corporation, a Lockheed Martin company, for the U.S. Department of Energy under Contract DE-AC04-94AL85000. The authors thank the Associate Editor, Prof. James Kubicki, a reviewer, Prof. Steve Parker, and two anonymous reviewers for their helpful comments on this manuscript.

Associate editor: James Kubicki

References

- Allen, M.P., Tildesley, D.J., 1987. *Computer Simulation of Liquids*. Oxford University Press, Oxford.
- Atkins, E.D.T., Nieduszy, I.A., Parker, K.D., 1973a. Structural components of alginic acid .1. crystalline—structure of poly-beta-D-mannuronic acid—Results of X-ray diffraction and polarized infrared studies. *Biopolymers* **12** (8), 1865–1878.
- Atkins, E.D.T., Nieduszy, I.A., Parker, K.D., Smolko, E.E., 1973b. Structural components of alginic acid .2. Crystalline—structure of poly-alpha-L-guluronic acid—Results of X-ray-diffraction and polarized infrared studies. *Biopolymers* **12** (8), 1879–1887.
- Banfield, J.F., Barker, W.W., Welch, S.A., Taunton, A., 1999. Biological impact on mineral dissolution: application of the lichen model to understanding mineral weathering in the rhizosphere. *Proc. Natl. Acad. Sci. USA* **96** (7), 3404–3411.
- Belitz, H., Grosch, W., 1987. *Food Chemistry*. Springer, Berlin.
- Boyd, A., Chakrabarty, A.M., 1995. *Pseudomonas aeruginosa* biofilms—role of the alginate exopolysaccharide. *Journal of Industrial Microbiology* **15** (3), 162–168.
- Braccini, I., Grasso, R.P., Pérez, S., 1999. Conformational and configurational features of acidic polysaccharides and their interactions with calcium ions: a molecular modeling investigation. *Carbohydr. Res.*, 119–130.
- Braccini, I., Pérez, S., 2001. Molecular basis of Ca²⁺-induced gelation in alginates and pectins: the egg-box model revisited. *Biomacromolecules* **2**, 1089–1096.
- Christensen, B.E., Charaklis, W.G., 1990. Physical and chemical properties in biofilms. In: Charaklis, W.G., Marshall, K.C. (Eds.), *Biofilms*. Wiley.
- Cormack, A.N., Lewis, R.J., Goldstein, A.H., 2004. Computer simulation of protein adsorption to a material surface in aqueous solution: biomaterials modeling of a ternary system. *J. Phys. Chem. B* **108** (52), 20408–20418.
- Cygan, R.T., 2001. Molecular modeling in mineralogy and geochemistry. In: Cygan, R.T., Kubicki, J.D. (Eds.), *Molecular Modeling Theory: Applications in the Geosciences*, vol. 42. Mineralogical Society of America, pp. 1–35.
- Dauber-Osguthorpe, P., Roberts, V.A., Osguthorpe, D.J., Wolff, J., Genest, M., Hagler, A.T., 1988. Structure and energetics of ligand-binding to proteins: *Escherichia coli* dihydrofolate reductase trimethoprim, a drug-receptor system. *Proteins Struct. Funct. Genet.* **4**(1), 31–47.
- Davis, T.A., Llanes, F., Volesky, B., Mucci, A., 2003. Metal selectivity of *Sargassum* spp. and their alginates in relation to their alpha-L-guluronic acid content and conformation. *Environ. Sci. Technol.* **37** (2), 261–267.
- de Leeuw, N.H., Cooper, T.G., 2004. A computer modeling study of the inhibiting effect of organic adsorbates on calcite crystal growth. *Crystal Growth Des.* **4** (1), 123–133.
- de Leeuw, N.H., Parker, S.C., 1997. Atomistic simulation of the effect of molecular adsorption of water on the surface structure and energies of calcite surfaces. *J. Chem. Soc. Faraday Trans.* **93** (3), 467–475.
- de Leeuw, N.H., Parker, S.C., Rao, K.H., 1998. Modeling the competitive adsorption of water and methanoic acid on calcite and fluorite surfaces. *Langmuir* **14** (20), 5900–5906.
- Delley, B., 1990. An all-electron numerical method for solving the local density functional for polyatomic molecules. *J. Chem. Phys.* **92** (1), 508–517.
- Delley, B., 2000. From molecules to solids with the DMol³ approach. *J. Chem. Phys.* **113**, 7756–7764.
- Dheu-Andries, M.L., Pérez, S., 1983. Geometrical features of calcium-carbohydrate interactions. *Carbohydr. Res.* **124** (2), 324–332.
- Didymus, J.M., Oliver, P., Mann, S., DeVries, A.L., Hauschka, P.V., Westbroek, P., 1993. Influence of low-molecular-weight and macro-molecular organic additives on the morphology of calcium carbonate. *J. Chem. Soc. Faraday Trans.* **89** (15), 2891–2900.
- Duckworth, O.W., Cygan, R.T., Martin, S.T., 2003. Linear free energy relationships between dissolution rates and molecular modeling energies of rhombohedral carbonates. *Langmuir* **20**, 2938–2946.
- Duffy, D.M., Harding, J.H., 2004. Simulation of organic monolayers as templates for the nucleation of calcite crystals. *Langmuir* **20** (18), 7630–7636.
- Effenberger, H., Mereiter, K., Zemmann, J., 1981. Crystal structure refinements of mangesite, calcite, rhodochrosite, siderite, smithsonite, and dolomite, with discussion of some aspects of the stereochemistry of calcite type carbonates. *Zeitschr. Kristallographie*. **156**, 233–243.
- Emmerichs, N., Wingender, J., Flemming, H.-C., Mayer, C., 2004. Interaction between alginates and manganese cations: identification of preferred cation binding sites. *Int. J. Biol. Macromol.* **34**, 73–79.
- Evans, L.R., Linker, A., 1973. Production and characterization of the slime exopolysaccharide of *Pseudomonas aeruginosa*. *J. Bacteriol.* **116**, 915–924.
- Fa, K.Q., Nguyen, A.V., Miller, J.D., 2005. Hydrophobic attraction as revealed by AFM force measurements and molecular dynamics simulation. *J. Phys. Chem. B* **109** (27), 13112–13118.
- Geissbühler, P., Fenter, P., DiMasi, E., Srajer, G., Sorensen, L.B., Sturchio, N.C., 2004. Three-dimensional structure of the calcite-water interface by surface X-ray scattering. *Surf. Sci.* **573**, 191–203.
- Grant, G.T., Morris, E.R., Rees, D.A., Smith, P.J.C., Thom, D., 1973. Biological Interactions between polysaccharides and divalent cations—egg-box model. *FEBS Lett.* **32** (1), 195–198.
- Guenot, J., Kollman, P.A., 1992. Molecular dynamics studies of a DNA-binding protein. 2. An evaluation of implicit and explicit solvent models for the molecular dynamics simulation of the *Escherichia coli* Trp repressor. *Protein Sci.* **1** (9), 1185–1205.
- Guimarães, C.R.W., Barreiro, G., de Oliveira, C.A.F., de Alencastro, R.B., 2004. On the application of simple explicit water models to the simulations of biomolecules. *Braz. J. Phys.* **34** (1), 126–136.
- Halgren, T.A., 1992. Representation of van der Waals (vdW) interactions in molecular mechanics force fields: potential form, combination rules, and vdW parameters. *J. Am. Chem. Soc.* **114** (20), 7827–7843.
- Hardalo, C., Edberg, S.C., 1997. *Pseudomonas aeruginosa*: assessment of risk from drinking water. *Crit. Rev. Microbiol.* **23** (1), 47–75.
- Haug, A., Myklesta, S., Larsen, B., Smidsrød, O., 1967. Correlation between chemical structure and physical properties of alginates. *Acta Chem. Scand.* **21** (3), 768.
- Hoog, C., Rotondo, A., Johnston, B.D., Pinto, B.M., 2002. Synthesis and conformational analysis of a pentasaccharide corresponding to the cell-wall polysaccharide of the Group A *Streptococcus*. *Carbohydr. Res.* **337** (21–23), 2023–2036.
- Hoover, W.G., 1985. Canonical dynamics: equilibrium phase-space distributions. *Phys. Rev. A* **31** (3), 1695–1697.
- Hwang, S., Blanco, M., Goddard, W.A., 2001. Atomistic simulations of corrosion inhibitors adsorbed on calcite surfaces I. Force field parameters for calcite. *J. Phys. Chem. B* **105**, 10746–10752.
- Iyer, L.K., Qasba, P.K., 1999. Molecular dynamics simulation of α -lactalbumin and calcium binding c-type lysozyme. *Protein Eng.* **12** (2), 129–193.
- Jamialahmadi, M., Mullersteinhagen, H., 1991. Reduction of calcium-sulfate scale formation during nucleate boiling by addition of EDTA. *Heat Transfer Eng.* **12** (4), 19–26.
- Kennedy, A.F.D., Sutherland, I.W., 1987. Analysis of bacterial exopolysaccharides. *Biotechnol. Appl. Biochem.* **9**, 12–19.
- Kerisit, S., Parker, S.C., 2004a. Free energy of adsorption of water and calcium on the {10-14} calcite surface. *Chem. Commun.*, 52–53.
- Kerisit, S., Parker, S.C., 2004b. Free energy of adsorption of water and metal ions on the {10-14} calcite surface. *J. Am. Chem. Soc.* **126**, 10152–10161.
- Kollman, P.A., 1996. Advances and continuing challenges in achieving realistic and predictive simulations of the properties of organic and biological molecules. *Acc. Chem. Res.* **29** (10), 461–469.

- Lattner, D., Flemming, H.-C., Mayer, C., 2003. ^{13}C -NMR study of the interaction of bacterial alginate with bivalent cations. *Int. J. Biol. Macromol.* **33**, 81–88.
- Martin, J.P., 1971. Decomposition and binding action of polysaccharides in soil. *Soil Biol. Biochem.* **3**, 33–41.
- Moore, R.E., Brenneman, D.R., Bischof, A.E., Robins, J.D., 1972. One-step anhydrite scale removal. *Mater. Prot. Perform.* **11** (3), 41–48.
- Perdew, J.P., Wang, Y., 1992. Accurate and simple analytic representation of the electron-gas correlation energy. *Phys. Rev. B: Condensed Matter* **45** (23), 13244–13249.
- Perry IV, T.D., Duckworth, O.W., McNamara, C.J., Martin, S.T., Mitchell, R., 2004. Effects of the biologically produced polymer alginic acid on macroscopic and microscopic calcite dissolution rates. *Environ. Sci. Technol.* **38**, 3040–3046.
- Pilson, M., 1998. *An Introduction to the Chemistry of the Sea*. Prentice-Hall, Englewood Cliffs, NJ.
- Reeder, R.J., Nugent, M., Tait, C., Morris, D., Heald, S., Beck, K., Hess, W., Lazirotti, A., 2001. Coprecipitation of uranium(VI) with calcite: XAFS, micro-XAS, and luminescence characterization. *Geochim. Cosmochim. Acta* **65**, 3491–3503.
- Rosseinsky, D.R., 1965. Electrode potentials and hydration energies: theories and correlations. *Chem. Rev.* **65**, 467–490.
- Saiz-Jimenez, C., 1999. Biogeochemistry of weathering processes in monuments. *Geomicrobiol. J.* **16**, 27–37.
- Schlesinger, W.H., 1997. *Biogeochemistry: An Analysis of Global Change*. Academic Press, New York.
- Smidsrød, O., Haug, A., 1965. Effect of divalent metals on properties of alginate solutions. I. Calcium ions. *Acta Chem. Scand.* **19** (2), 329.
- Stahl, G., Patzay, G., Weiser, L., Kalman, E., 2000. Study of calcite scaling and corrosion processes in geothermal systems. *Geothermics* **29**, 105–119.
- Stockelmann, E., Hentschke, R., 1999. Adsorption isotherms of water vapor on calcite: a molecular dynamics-Monte Carlo hybrid simulation using a polarizable water molecule. *Langmuir* **15** (15), 5141–5149.
- Stumm, W., 1992. *Chemistry of the Solid–Water Interface*. Wiley.
- Stumm, W., Morgan, J.J., 1996. *Aquatic Chemistry*. Wiley.
- Sun, H., Ren, P., Fried, J.R., 1998. The COMPASS force field: parameterization and validation for phosphazenes. *Comput. Theoret. Polym. Sci.* **8** (1–2), 229–246.
- Thomas, M., Clouse, J., Longo, J., 1993. Adsorption of organic compounds on carbonate minerals 3. Influence on dissolution rates. *Chem. Geol.* **109**, 227–237.
- Tosi, M.P., 1964. Cohesion of ionic solids in the Born model. *Solid State Phys.* **131**, 533–545.
- Verlet, L., 1967. Computer ‘experiments’ on classical fluids: I. Thermodynamical properties of Lennard–Jones molecules. *Phys. Rev. A* **195**, 98–103.
- Welch, S.A., Barker, W.W., Banfield, J.F., 1999. Microbial extracellular polysaccharides and plagioclase dissolution. *Geochim. Cosmochim. Acta* **63** (9), 1405–1419.
- Welch, S.A., Vandevivere, P., 1994. Effect of microbial and other naturally occurring polymers on mineral dissolution. *Geomicrobiol. J.* **12**, 227–238.
- Whitting, S., 1971. Conformational energy calculations on alginic acid. 1. Helix parameters and flexibility of homopolymers. *Biopolymers* **10** (9), 1481–1489.
- Wolfgang, M.C., Kulasekara, B.R., Liang, X.Y., Boyd, D., Wu, K., Yang, Q., Miyada, C.G., Lory, S., 2003. Conservation of genome content and virulence determinants among clinical and environmental isolates of *Pseudomonas aeruginosa*. *Proc. Natl. Acad. Sci. USA* **100** (14), 8484–8489.